

ACCEPTED MANUSCRIPT



Mapping the functional versatility and fragility of Ras GTPase signaling circuits through *in vitro* network reconstitution

Scott Coyle, Wendell A Lim

DOI: <http://dx.doi.org/10.7554/eLife.12435>

Cite as: eLife 2016;10.7554/eLife.12435

Received: 20 October 2015

Accepted: 13 January 2016

Published: 14 January 2016

This PDF is the version of the article that was accepted for publication after peer review. Fully formatted HTML, PDF, and XML versions will be made available after technical processing, editing, and proofing.

Stay current on the latest in life science and biomedical research from eLife.
[Sign up for alerts](#) at elife.elifesciences.org

1

2

3

4

5

6 **Mapping the functional versatility and fragility of Ras GTPase
7 signaling circuits through *in vitro* network reconstitution**

8

9 Scott M. Coyle¹⁻³, Wendell A. Lim^{1-3*}

10

11

12 ¹Howard Hughes Medical Institute and Department of Cellular & Molecular
13 Pharmacology, University of California San Francisco, San Francisco, CA 94158, USA

14 ²Program in Biological Sciences

15 ³UCSF Center for Systems and Synthetic Biology

16 *To whom correspondence should be addressed: lim@cmp.ucsf.edu

17

18

19 **Abstract**

20 The Ras-superfamily GTPases are central controllers of cell proliferation and morphology. Ras
21 signaling is mediated by a system of interacting molecules: upstream enzymes (GEF/GAP)
22 regulate Ras's ability to recruit multiple competing downstream effectors. We developed a
23 multiplexed, multi-turnover assay for measuring the dynamic signaling behavior of *in vitro*
24 reconstituted H-Ras signaling systems. By including both upstream regulators and downstream
25 effectors we can systematically map how different network configurations shape the dynamic
26 system response. The concentration and identity of both upstream and downstream signaling
27 components strongly impacted the timing, duration, shape and amplitude of effector outputs.
28 The distorted output of oncogenic alleles of Ras was highly dependent on the balance of
29 positive (GAP) and negative (GEF) regulators in the system. We found that different effectors
30 interpreted the same inputs with distinct output dynamics, enabling a Ras system to encode
31 multiple unique temporal outputs in response to a single input. We also found that different
32 Ras-to-GEF positive feedback mechanisms could reshape output dynamics in distinct ways,
33 such as signal amplification or overshoot minimization. Mapping of the space of output
34 behaviors accessible to Ras provides a design manual for programming Ras circuits, and
35 reveals how these systems are readily adapted to produce an array of dynamic signaling
36 behaviors. Nonetheless, this versatility comes with a trade-off of fragility, as there exist
37 numerous paths to altered signaling behaviors that could cause disease.

38

39 **Introduction**

40 Many dynamic processes in the cell such as proliferation, differentiation or morphological
41 change are regulated by signaling through members of the Ras superfamily of small GTPases
42 (1–5). Mutations in these important molecules are often associated with cancer or other
43 diseases (6, 7). These small GTPases act as macromolecular “switches” at cell membranes,
44 cycling between an ON state when bound to GTP and an OFF state when bound to GDP (5)
45 (**Figure 1A**). This notion of an ON and OFF state of the GTPase is manifest in differences in the
46 conformation of the protein such that, in most cases, only the GTP-bound state is able to
47 interact with downstream effector molecules and assemble signaling complexes (8–11).

48 As enzymes, these GTPases are formally capable of binding GTP, hydrolyzing it to GDP+P_i,
49 and releasing product to complete the catalytic cycle on their own, but in practice the GTPase is
50 incredibly slow at each stage of this cycle except for the initial binding of nucleotide (12–14). As
51 such, molecules that can accelerate these slow steps in the catalytic cycle function as essential
52 regulators of GTPase activity during signaling events: guanine exchange factors (GEFs), which
53 promote product release by emptying the nucleotide pocket of the GTPase and allowing
54 subsequent reloading of the GTPase with nucleotide (OFF->ON transition); and GTPase
55 activating proteins (GAPs) which accelerate the hydrolysis of GTP to GDP+P_i (ON->OFF
56 transition) (**Figure 1A**) (15–18). How Ras processes information, then, is not determined by Ras
57 alone, but rather is also highly dependent on a system of molecules comprising the upstream
58 GEFs and GAPs that regulate its activity, and the downstream effector molecules that are
59 engaged and regulated by the activated GTPase (**Figure 1B**).

60 Our biochemical view of Ras and Ras associated proteins, however, is largely focused on
61 individual molecules, rather than the system of molecules. Considerable work *in vitro* over
62 several decades has provided structural and biochemical insights into how individual GEFs,
63 GAPs and effectors function, as well as how their activity can be controlled through mechanisms
64 like autoinhibition and allostery (19–26). These studies have provided many of the most
65 fundamental insights into the mechanisms of Ras activation and inactivation as well as clarified
66 our understanding of the nature of oncogenic mutations. To study the regulators, however,
67 these reconstitutions are almost always performed under conditions in which Ras cannot
68 productively cycle: GEF assays monitor a single exchange of fluorescent nucleotide for non-
69 fluorescent nucleotide; GAP assays monitor a single turnover of GTP without the possibility of
70 the nucleotide reloading (27). Likewise, studies of effector interactions with activated GTPase

71 are typically done under non-cycling conditions using non-hydrolyzable nucleotide analogs to
72 measure equilibrium binding constants (28–30). However, we know that signaling dynamics are
73 critical for many cellular responses, and yet these features have not been analyzed in most *in*
74 *vitro* studies of Ras signaling.

75 By comparison, cell-based investigations of signaling are inherently multi-component and multi-
76 turnover with respect to Ras, but provide far less control over the internal system parameters. *In*
77 *vivo* assays usually contain fewer observables that are often far removed from the proximal
78 signaling events. A variety of ingenious experiments have aimed to directly probe Ras activation
79 during signaling in cells using fluorescent reporter molecules or super-resolution microscopy
80 (31–33). However, the complications of using these reporter tools in living cells have made it
81 difficult to systematically probe the behavior of the Ras signaling module. For example it is
82 difficult to know whether the response of one FRET reporter represents that of the diverse Ras
83 effector species in the cell.

84 To date, there has been little *systems reconstitution* of Ras signaling – methodically exploring *in*
85 *vitro* how the multiple activities that regulate Ras work together to dynamically cycle Ras and
86 control the assembly of competing effectors on activated Ras during signal processing. As such,
87 we know little about how the concentration and identity of the components within a Ras system
88 define its signaling properties. Understanding how these systems-level parameters shape
89 behavior is critical, given that different cell types can harbor different configurations of network
90 components (both in identity and expression levels) and also because distinct receptors may
91 differentially activate key network components. In addition, the fact that many diseases are
92 associated with perturbations to Ras and its associated regulators suggests that a systems level
93 reconstitution of Ras signaling systems could be highly informative as to types of outputs and
94 behaviors that these systems are capable of, as well as how these systems respond to
95 perturbations such as mutation.

96 Here, to address this problem of systems reconstitution, we develop a new microscopy-based
97 bead reconstitution assay of dynamic signal processing by human H-Ras, a canonical member
98 of the Ras subfamily of GTPases. Our system includes both upstream regulators of Ras activity
99 as well as multiple downstream effectors that bind to and perceive Ras•GTP signals. This allows
100 us to follow multiple cycles of Ras turnover in real-time using the bead recruitment of
101 fluorescently tagged effectors on Ras as the measured output – precisely analogous to the way
102 cells measure and couple Ras•GTP levels to signaling outputs. In addition to giving an output

103 that reflects a critical biological function (effector recruitment), this system allows us to precisely
104 control the components and their concentration.

105 Using this system we have explored how Ras signaling changes in response to network
106 changes. We explore how oncogenic substitutions in Ras impact output behavior. We have
107 scanned how the concentration of each type of network component sculpts effector outputs in
108 response to a simple step input of GEF activity, how systems that contain multiple competing
109 effector molecules behave, and how different mechanisms for implementing positive feedback
110 reshape the landscape of output behaviors. More generally, the methods we develop herein
111 provide a framework for studying the dynamics of other assembly driven signaling systems or
112 more complex systems that incorporate multiple interconnected signaling nodes. This kind of
113 analysis provides an overall design manual for Ras circuits, including those that could have
114 originated through evolution or disease perturbation.

115

116 **Results**

117 **Systems-level reconstitution of Ras signal processing *in vitro*: tracking effector output 118 dynamics across multiple GTPase turnovers**

119 To gain insight into the dynamics of how Ras transmits signals to downstream effectors under
120 different network configurations or perturbations, we sought a dynamic *in vitro* reconstitution of
121 Ras signal processing that would allow us to track effector outputs across multiple Ras
122 turnovers. We reasoned that a microsphere surface charged with Ras could serve as a platform
123 for the assembly and disassembly of fluorescent effector molecules from solution in response to
124 inputs, much like the native Ras system (bound to the plasma membrane) functions in cells
125 (**Figure 2A**). Signaling networks of defined composition could then be prepared from
126 recombinant proteins and robust measurements of the dynamic output behavior could be
127 determined by tracking the amount of effector on the surface over time for many individual
128 beads and averaging their responses. Though such a system would not fully capture all
129 biophysical features of cellular Ras signaling, such as GTPase diffusion in a fluid plasma
130 membrane, partitioning between membrane microdomains, or GTPase exchange from the
131 membrane, it serves as an excellent starting point to understand how these systems behave
132 with fixed Ras molecules in a highly controlled setting (34, 35). Moreover, although the signaling
133 activity of most Ras effectors is more complex than binding alone (see, for example: 36, 37), the
134 regulated interaction of effectors with GTPase is the foundation on which any other complex

135 signaling mechanisms will unfold, and thus represents a universal and fundamental feature of all
136 Ras signaling systems that demands our understanding.

137 We first asked whether we could observe GTP-dependent translocation of an effector molecule
138 to a Ras-coated bead catalyzed by a guanine nucleotide exchange factor (GEF). For our initial
139 studies, we chose to use the catalytic domain from the RasGRF GEF, which is constitutively
140 active and, unlike other GEFs, contains no allosteric feedback sites (38). Ni-NTA microspheres
141 were charged with a 16x-histidine tagged H-Ras•GDP (OFF state) that could not dissociate from
142 the bead and incubated in the presence of 50 nM ($\sim K_D$) of a model effector: a fluorescently
143 tagged Ras-binding domain (RBD) from the C-Raf kinase (39). Under these basal conditions,
144 the amount of fluorescence on the bead was comparable to the background levels of
145 fluorescence from the effector in solution. We then added as input 2 μ M of the catalytic domain
146 of the RasGRF GEF and 5 mM of either GDP or GTP and monitored the output of effector
147 fluorescence on the bead (**Figure 2B**). This amount of nucleotide in solution is in vast excess of
148 the small amount of bead-bound Ras present in the reactions, providing essentially an infinite
149 supply of nucleotide for these reactions on the timescale we examine (detailed in Materials and
150 methods). Upon GEF and nucleotide addition, there was noticeable accumulation of fluorescent
151 effector on the bead surface of the GTP containing reactions within seconds, and considerable
152 fluorescent signal was observed by ten minutes. In contrast, no fluorescent effector
153 accumulated on the surface of reactions containing GDP, indicating that GEF-catalyzed
154 translocation of the effector was dependent on Ras becoming GTP loaded. Having seen GTP-
155 dependent GEF-catalyzed translocation of an effector to a Ras-charged bead surface, we were
156 now in position to prepare signaling networks of arbitrary configuration and assay their output
157 dynamics in multiplex using our microscopy based assay (**Figure 2C**).

158 We first asked whether we could observe *quantitative* differences in the system's output
159 behavior when different amounts of GEF activity were used as inputs. When identically loaded
160 beads were stimulated with increasing amounts of RasGRF, we observed both faster rates of
161 effector translocation and higher steady state amplitudes of effector output (**Figure 2D, Figure**
162 **2-figure supplement 1A-B**). Initial rates of effector translocation appeared to show a hyperbolic
163 response to increasing GEF, while steady states effector levels showed a linear response.
164 Together, these data demonstrate that our reconstituted Ras signal processing system
165 produced outputs that responded quantitatively to the amount of GEF present in the system.

166 In addition to being able to turn on, a *dynamic* reconstitution of Ras signal processing must be
167 reversible and be able to turn off. To test the reversibility and turn-off of our system, we

168 prepared beads loaded with H-Ras•GTP (ON state), incubated them with a saturating excess
169 amount of C-Raf RBD effector (2.5 μ M total, 50 nM fluorescently labeled), and monitored the
170 loss of effector signal from the bead over time (**Figure 2E**). In the absence of any GTPase
171 activating protein (GAP), effector fluorescence decayed with a rate constant of 0.01 min⁻¹, which
172 is similar to the expected rate of intrinsic hydrolysis by H-Ras under our assay conditions (12,
173 13). This result is consistent with previous observations that intrinsic hydrolysis by the GTPase
174 continues to occur even in the presence of saturating amounts of effector (40). When
175 increasing amounts of the catalytic domain from purified Neurofibromin-1 GAP (NF1-GAP (41,
176 42)) were included in the reactions, effector signal disappeared from the bead at an increased
177 rate in a dose-dependent manner with a hyperbolic dependence on the GAP concentration
178 (**Figure 2E, Figure 2-figure supplement 1C**). Thus, as with the turn-on of the system, these
179 data indicate that our reconstituted Ras signal processing system displays turn-off that responds
180 quantitatively to the amount of GAP present in the system.

181 Having found that our system can produce effector outputs that are turned on by GEF and
182 turned off by GAP, we wanted to verify that the system was truly multi-turnover and that the
183 output dynamics would respond to both of these activities working in concert. To this end, we
184 incubated Ras•GDP loaded beads with 50 nM fluorescent effector, initiated signaling with 2 μ M
185 RasGRF GEF and 5 mM GTP, and then added 1 μ M NF1-GAP at 25 minutes (**Figure 2F**). As
186 before, addition of GEF stimulated assembly of effector on the bead as the levels of Ras•GTP
187 increased. When NF1-GAP was added to the reactions, the system responded with a rapid
188 decrease in effector levels before stabilizing at a non-zero plateau corresponding to the non-
189 equilibrium steady state maintained by the balance of effector, GEF and GAP activities present
190 in the reaction.

191 Taken together, these data imply that our on bead reconstitution of H-Ras signal processing can
192 semi-quantitatively track dynamic effector outputs across multiple cycles of Ras activation and
193 deactivation during signaling. This system now puts us in position to explore how different
194 mutational states, network configurations, protein identities or feedback mechanisms affect
195 signal processing by Ras GTPase systems.

196

197 **Distortion of signaling by oncogenic Ras alleles depends on balance of positive and**
198 **negative regulatory activities in the network.** Mutations of Ras (especially at the G12, G13, or
199 Q61 positions) are frequently associated with cancer or other diseases (43). These alleles are

200 primarily thought to impact Ras signaling through three mechanisms: 1) decreasing the intrinsic
201 hydrolysis rate of the GTPase, 2) blocking GAP-mediated hydrolysis of the GTPase, and 3)
202 potentially altering the interaction and preference of the GTPase for downstream effectors
(Figure 3A) (16, 43–45). The same mutant allele of Ras can elicit different phenotypes in
204 different cell types and tissues. Thus we wanted to use our *in vitro* systems reconstitution assay
205 to determine which system configurations are most sensitive to these oncogenic perturbations.

206 Using our dynamic, multi-turnover reconstitution of Ras signal processing, we examined how
207 signaling networks bearing the G12V allele of the Ras GTPase distorted effector outputs relative
208 to the wildtype Ras GTPase. By labeling wildtype and G12V Ras GTPases with different
209 fluorophores, we could distinguish beads loaded with each variant in a common solution of
210 network components to see differences in effector outputs from each system side-by-side.

211 For these and future experiments, we display the output response data in two ways: (1) we
212 show the absolute response, which conveys information about both the *amplitude and the shape*
213 of the output response, and (2) we show the responses after normalizing to the maximum
214 value of the response, which conveys information *only about the shape* or dynamic profile of the
215 output. The latter is particularly useful for seeing how the shape of two responses differs when
216 the amplitudes are substantially different.

217 With this approach, we first examined the output of 50 nM C-Raf RBD effector from G12V or
218 wildtype Ras networks *without* GAP activity in response to a step input of 2 μ M of the GEF
219 RasGRF (**Figure 3B, Video1**). Under this network configuration, wildtype and G12V Ras
220 systems produced very similar outputs with almost no difference in the total integrated effector
221 output and only small differences in the overall dynamics of their responses. This suggests that
222 neither the intrinsic hydrolysis nor changes in C-Raf RBD effector interactions of the G12V
223 substitution are particularly perturbative to the output of the signaling system under this GAP-
224 free network configuration.

225 We then looked at the system responses of wildtype and G12V Ras systems to the exact same
226 step-input (2 μ M RasGRF GEF) but in networks that now included 1 μ M basal NF1-GAP
227 (**Figure 3C, Video2**). Unlike in the GEF-only networks, both the dynamics and amplitude of the
228 effector output were substantially distorted by the Ras-G12V allele. In this network
229 configuration, wildtype Ras produced a *transient* response that peaked within an hour and
230 declined to a steady state less than 20% its maximum value. In contrast, outputs from G12V
231 were sustained and increased in magnitude for over 6 hours before settling at a steady state

232 more than 40 times higher than wildtype Ras. Thus, the G12V mutation is significantly
233 perturbative in a high-GAP network context.

234 Together these data and model imply that the balance of positive and negative regulatory
235 activities in a signaling network impacts the severity by which Ras-G12V distorts signals. Similar
236 results were also observed for G12C and Q61L alleles (**Figure 3-figure supplement 1**). To
237 determine which particular configurations are most distorted by the G12V allele, we measured
238 the effector output response across 4 different input strengths ([GEF] activity) and 4 different
239 NF1-GAP levels. We then calculated a distortion score as the fold-change integrated output
240 from Ras-G12V relative to wildtype Ras and interpolated the responses from these 16
241 configurations to produce a phase diagram of signal distortion by G12V under different network
242 conditions (**Figure 3D**). This revealed that G12V alleles were most perturbative with low-GEF
243 inputs and a high-GAP network context, conditions in which the GAP activity would, for wildtype
244 Ras, completely dominate over the small amount of activating GEF input. These observations
245 are consistent with models of oncogenic Ras signaling in which low-level inputs or noise from
246 the environment that would normally be filtered out by basal GAP-activity are misinterpreted by
247 the cell as *bona fide* activating signals.

248

249 *Modeling suggests competition and intermediates contribute to transient signaling dynamics of*
250 *wildtype Ras-GTPase systems in contrast to oncogenic variants.*

251 The transient response of the wildtype GTPase in the high-GAP network context was
252 unanticipated, as this phenomenon cannot be explained by the simplest model of
253 effector/GTPase binding in which the GTPase toggles ON and OFF with rates directly
254 proportional to [GAP] and [GEF] (Figure 3-figure supplement 2). Indeed, this is consistent with
255 analytic results that state that two-state systems cannot show overshoot behavior (46).
256 However, transient overshoot could be easily introduced into the system by two non-mutually
257 exclusive mechanisms: (1) competition between effectors and GAP molecules; and (2) the
258 existence of a post-hydrolysis GTPase state that is refractory to GEF stimulation.

259 We found that extending the two-state model to include competition could produce overshoot,
260 but this required higher concentrations of the Raf-RBD effector than the GAP and tighter binding
261 of GAP to GTPase than Raf-RBD to GTPase, neither of which are consistent with the known
262 parameters of the system (Figure 3-figure supplement 2). Moreover, because GAP can bind

263 (but not stimulate the hydrolysis of) the G12V, competition cannot explain the differences we
264 observed between the wildtype and G12V dynamics.

265 In contrast, the introduction of a refractory GTPase state to the model produced overshoot that
266 captured the key features of the observed data within physiological parameters: a monotonic
267 response to inputs in low-GAP networks but a transient response in high-GAP networks (Figure
268 3-figure supplement 2). It also is consistent with the differences in dynamics that we observed
269 between G12V and wildtype Ras. While the exact molecular nature of this intermediate
270 GTPase state is not clear at present, this does not hinder our ability to study its consequences
271 for signal processing.

272

273 **Concentration and identity of Ras network components modulates timing, duration,
274 shape, and amplitude of effector outputs.**

275 Our comparison of wildtype and G12V Ras signaling systems and our associated model
276 illustrated the importance of the network composition in shaping signal processing outputs.
277 Each individual network component is, in essence, a separate “dial” of the Ras signaling system
278 that can be turned by adjusting the concentration of that component (**Figure 4A**). Because
279 expression levels of signaling components vary across different cell types and are often different
280 in oncogenic states, we wondered how the level of each network component impacted signal
281 processing wildtype Ras signaling networks. To this end, we fixed a particular input (2 μ M
282 RasGRF GEF) and, starting from a particular initial system configuration (~2500 Ras molecules
283 \times μ m 2 , 50 nM C-Raf effector, no GAP activity) with an associated output response, asked how
284 titration of individual system components modulated the effector output.

285 *Effects of GAP Activity: the properties of distinct GAP species*

286 Having seen dramatic effects of negative regulatory activities in our distortion analysis of G12V
287 Ras, we first looked more generally at how GAP activity sculpted signal processing dynamics in
288 wildtype Ras networks. We considered two distinct GAPs domains with different biochemical
289 properties and expression patterns: the NF1-GAP and the p120-GAP. NF1-GAP, which is
290 expressed somewhat ubiquitously but highest in neuronal cells and leukocytes, has a tight K_M
291 for Ras (0.3 μ M) and modest k_{cat} (1.4 s $^{-1}$) (47). In contrast, p120GAP has a higher K_M (9.7 μ M)
292 for Ras, but also a higher k_{cat} (19 s $^{-1}$), and shows a much more ubiquitous expression profile
293 (47).

When increasing amounts of NF1-GAP were included in networks, the same step input of GEF activity produced dramatically different effector output behaviors (**Figure 4B**). First, increasing levels of NF1-GAP resulted in substantially lower end point steady state levels of bound effector. Moreover, the amount of NF1-GAP changed the *dynamics of approach* to steady state significantly: while GAP-free networks approached steady state from below, networks containing NF1-GAP showed transient overshoot that decayed back down to the steady state from above, creating an initial pulse of strong output followed by weaker levels of output in the long term. The pulse-width and peak-time of effector outputs were inversely correlated with the concentration of the NF1-GAP (**Figure 4B**). Thus, NF1-GAP shapes not only the final steady-state levels of output in the system, but also the shape, timing and duration of Ras signal processing.

As discussed previously in the context of our initial kinetic model, overshoot dynamics such as these are a hallmark of energetically-driven chemical systems that contain *more* than two states approaching a non-equilibrium steady-state, in which intermediate system states can transiently accumulate and then de-accumulate as the system begins to cycle (46, 48, 49). This is analogous to the way in which enzyme intermediates can transiently accumulate in the pre-steady state depending on the rate-constants for the microscopic steps, for example if product release is rate-limiting (50). Our observation of these phenomena in Ras circuits is only possible because our system uses *bona fide* GTP that allows for Ras cycling to actively occur. Consistent with this, the G12V, G12C, and Q61L mutants we analyzed previously – which cannot efficiently cycle – did not show such overshoot behavior even under the highest GAP conditions examined.

We repeated this analysis using the catalytic domain of p120GAP in our networks instead of NF1-GAP. Compared to the NF1-GAP, the impact of the p120GAP on the end-point effector output of the system was much less substantial (**Figure 4C**). This may in part be owing to the much higher K_M of p120GAP compared to NF1-GAP, leading to much lower effective GAP activity in the concentration regimes we could readily explore. Nonetheless, increasing amounts of p120GAP levels did lead to a marked change in the output dynamics of Ras signal processing in a manner similar to that of NF1-GAP, and is consistent with the consequences of altering the K_M and k_{cat} of the GAP in our kinetic model (Figure 5-figure supplement 3). As with NF1-GAP, transient behaviors emerged when p120GAP was present, and the pulse-width and peak-time of effector outputs were inversely correlated with the concentration of p120GAP. Thus, like NF1-GAP, p120GAP shapes the dynamics and steady-state behavior of signal

327 processing by Ras, but with a different dose-dependent behavior owing to its unique
328 biochemical characteristics.

329

330 *Effects of Ras Density: how expression level and clustering can alter signaling*

331 Given that Ras expression level can vary among different cell-types and that Ras distribution in
332 the plasma membrane can be both free as well as packed into high-density nanoclusters (51,
333 52), the next system parameter we considered was the density of Ras. We made a dilution
334 series of Ras, loaded beads with each dilution, and then mixed these beads together to assay
335 the responses of different Ras densities side-by-side in the exact same network solution.
336 Because the Ras was fluorescently labeled, we could estimate the Ras density from the
337 intensity of each bead and bin the responses from similar density beads together to obtain
338 average behaviors for different density classes.

339 Applying this approach to our fixed step-input, we found that the Ras density was directly
340 correlated with the amplitude of effector output produced by the system (**Figure 4D**). This is
341 expected as higher Ras densities provide more molecules that can form Ras•Effector
342 complexes. Additionally, the normalized traces of these responses revealed differences in the
343 dynamic behavior of effector output. When Ras densities were high, the step-response effector
344 output monotonically approached its steady state and was sustained.

345 At lower Ras densities, however, effector output responses were increasingly transient in
346 character. These outputs peaked early in the response and then decreased significantly to a
347 lower value over the time-course. These differences likely reflect a switch from a network
348 configuration in which Ras is in excess of the GEF to one in which the GEF is in excess of Ras,
349 and this idea is supported by our kinetic model (Figure 5-figure supplement 3). Intuitively, these
350 differences will cause a change the initial fraction of the Ras population that is activated, such
351 that a much larger synchronous cohort is formed at lower Ras densities.

352

353 *Effects of C-Raf RBD effector concentration: active roles for downstream components*

354 Finally, we considered the impact of the concentration of effectors, the molecules that are used
355 by cells to perceive and interpret Ras•GTP dynamics in the cell, on signal processing. For
356 these experiments, we fixed the amount of fluorescent C-Raf RBD effector at 50 nM and added
357 additional unlabeled C-Raf RBD to achieve a target final concentration of effector. We could

358 then normalize the observed fluorescent effector output by its proportion in the total effector
359 population to infer the true magnitude of the output.

360 When we measured the system step-response in the presence of increasing amounts of effector
361 in the network, dramatic changes in the both the amplitude and dynamics of output were
362 observed (**Figure 4E**). At an effector concentration of 50 nM ($\sim K_D$), the system output showed
363 the typical monotonic approach to a sustained steady-state.

364 When we increased effector concentrations, both the amplitude and the dynamics of the output
365 response changed markedly. At 250 nM effector concentration, output increased to a level 20
366 times that of the 50 nM effector system (measured at 120 min) at that time, before decaying
367 down to its final steady state level. At even higher effector concentrations (500 nM, 1000 nM),
368 system output peaked quickly within 20 minutes and then decayed monotonically over several
369 hours to the final steady state level. These data demonstrate that higher effector concentrations
370 not only increase output amplitudes, but also enable the output to capture more transient
371 features of the upstream Ras•GTP signal. This idea is supported by our kinetic model (Figure 5-
372 figure supplement 3) and makes sense intuitively because higher effector concentrations
373 decrease the time needed to equilibrate against a fixed concentration of Ras•GTP; if this
374 process is too slow, transient aspects of the GTPase activation/deactivation dynamics that
375 occur on a faster timescale will be missed in the effector output. This implies that effectors are
376 not merely passive conduits for transmitting upstream Ras dynamics, but instead play an active
377 role in interpreting and perceiving what features of those dynamics to pass downstream during
378 signaling. A corollary of this observation is that erroneous overexpression of effector molecules
379 can not only lead to higher amplitude outputs, but can also drastically alter the overall dynamics
380 of the system behavior as well.

381

382 *Diverse dynamic outputs achieved by titration of components*

383 Our data show that the identity and concentration of each component in a Ras signaling network
384 can have a profound impact on the timing, duration, shape, or amplitude of effector outputs.
385 This implies by tuning the abundance and identity of network components and controlling the
386 strength of inputs, a variety of diverse dynamic effector output programs can be realized by Ras
387 signaling system (**Figure 5A**). To explore this space of output programs more thoroughly, we
388 fixed a particular effector concentration (50 nM, $\sim K_D$) and measured system output from
389 different Ras densities, p120GAP concentrations, and input strengths ([GEF]). In total, we

390 experimentally measured output responses for 96 configurations corresponding to 4 different
391 input strengths, 4 different GAP concentrations, and 6 different Ras densities (**Figure 5B**,
392 normalized responses in **Figure 5-figure supplement 1**).

393 The diversity of dynamic output responses we observe highlights the versatility and tunability of
394 the Ras signaling system: sustained responses of arbitrary amplitudes can be produced as well
395 as transient responses with different peak times and magnitudes of overshoot, all by simply by
396 co-varying the levels of different system parameters. Because the number of output responses
397 we measured is large, we extracted 3 features from each output response trace that describe
398 the behavior – integrated signal intensity, initial rate of activation, and a transient score that
399 reflect the amount of overshoot in the response – and interpolated these values for 3 different
400 Ras density bins to create an experimentally determined signal processing phase diagram for
401 each output feature as a function of the network configuration (**Figure 5-figure supplement 2**).

402 These phase-diagrams not only summarize the output responses we measure but also clarify
403 the structure of the space of Ras signaling behaviors. This provides a roadmap for
404 understanding how output responses change as we alter system parameters and helps predict
405 the impact of perturbations that move the system from one region of the space to another. The
406 isoclines in these diagrams also highlight the existence of different network configurations with
407 equivalent signaling behaviors. These correspond to neutral paths in network-space that the
408 signaling system can drift along without immediate consequence to signaling output.

409

410 **Different Ras effectors perceive the same input uniquely, enabling multiple distinct**
411 **temporal outputs to be encoded in multi-effector networks.**

412 So far our characterization of Ras signal processing has used the C-Raf RBD as the sole
413 downstream effector, but in living cells these networks typically contain *multiple* effectors
414 targeting *different* output responses that are in *competition* with one another for access to
415 activated Ras, with each of these effectors possessing its own affinity for Ras•GTP and
416 expression level in the cell (11, 45). Indeed, our kinetic modeling implied that competition was
417 another important source of dynamic complexity in these systems (Figure 3-figure supplement
418 2). Because our reconstituted signal processing is microscopy based, we can track the behavior
419 of multiple distinct competing effectors processing signals on the same bead simultaneously by
420 labeling each effector with a different color fluorophore (**Figure 6A**). To this end, we purified and
421 labeled Ras-binding domains from the A-Raf and B-Raf kinases, which have lower ($k_{off}=5.52\times 10^{-$

422 4 s $^{-1}$, $k_{on}=7.20\times10^3$ M $^{-1}$ s $^{-1}$) and higher ($k_{off}=1.48\times10^{-4}$ s $^{-1}$, $k_{on}=1.32\times10^4$ M $^{-1}$ s $^{-1}$) affinities for
423 Ras•GTP than C-Raf ($k_{off}=2.15\times10^{-4}$ s $^{-1}$, $k_{on}=1.02\times10^4$ M $^{-1}$ s $^{-1}$) respectively (53), to examine the
424 signal processing behavior of two-effector systems in either GAP-free or high NF1-GAP
425 networks.

426 We first considered networks containing equivalent, physiological amounts of C-Raf and B-Raf
427 effectors, which both have high affinity for Ras•GTP (45). In response to a 2 μM RasGRF GEF
428 step input in a GAP-free network, C-Raf and B-Raf processed these signals with different
429 amplitudes and completely different dynamics (**Figure 6B**). Initially C-Raf and B-Raf outputs
430 assembled at comparable rates, but within 1 hour C-Raf output peaked and began to decrease
431 while B-Raf continued to increase in output monotonically over the entire time course. When
432 these step-responses were re-examined in a high NF1-GAP network context, we continued to
433 see different effector responses between C-Raf and B-Raf: C-Raf output peaked within 30
434 minutes before sharply declining to a steady state value 25% of its maximum. In contrast, B-Raf
435 output peaked later at one hour, and declined to a 75% its peak maximum, a much higher
436 steady state compared to C-Raf (**Figure 6C**). Thus, in this case, one effector (B-Raf) produces
437 a transient response while a different effector (C-Raf) produces a more sustained output.

438 Why do different effector molecules interpret upstream Ras signals with different output
439 dynamics as we observed? Two factors contribute to this phenomenon. First, as we previously
440 saw with one-effector systems, the time it takes for a binding process to equilibrate impacts the
441 extent to which it can track the transient dynamics of its target. Distinct effector molecules have
442 different binding affinities that are determined by different on and off rates from the target, and
443 thus will interpret Ras dynamics differently. Second, these effector molecules are in competition
444 with one another for access to the supply of time-varying activated Ras. Because we are
445 observing the nonequilibrium binding dynamics of effectors to Ras, an effector may be
446 competitive in the short-term (kinetically-determined phase) but less so in the long-term
447 (equilibrium-determined phase) (54). Appropriately, the inclusion of competing effectors with
448 physiological parameters in our model produced dynamics recapitulating such different effector
449 responses (Figure 6-figure supplement 2).

450 We then performed a similar analysis for two-effector systems containing equivalent,
451 physiological amounts of C-Raf and A-Raf RBDs, where A-Raf has a weaker affinity for
452 Ras•GTP and higher off-rate from the GTPase than C-Raf (45). In GAP-free networks, the step-
453 responses for A-Raf and C-Raf differed most significantly in terms of their amplitudes, with A-
454 Raf output 20 times lower than C-Raf output (**Figure S5B**). The normalized traces of each

455 effector output show only minor differences in the dynamics of these outputs. In high NF1-GAP
456 networks, we could only detect an output response from the C-Raf effector; the ability of A-Raf
457 to assemble on the bead was either filtered out by the low affinity combined with high levels of
458 GAP activity, or was simply too weak to detect above the background A-Raf in solution (**Figure**
459 **6D**).

460 Clearly effector molecules with distinct identities result in differential interpretation of inputs, but
461 how easy is it for a given effector molecule to acquire a new dynamic behavior? Given that A-
462 Raf, B-Raf, and C-Raf have different affinities for the GTPase, we wondered whether mutations
463 in C-Raf that changed its affinity would be sufficient to drive new dynamic behaviors. To this
464 end, we characterized the step-response of two-effector network containing equivalent amounts
465 (50 nM) of the C-Raf RBD and the C-Raf^{N64A} point mutant that has decreased affinity for
466 Ras•GTP (39). Different dynamic output behaviors for each effector were observed for both
467 GAP-free (**Figure S5C**) and high NF1-gap (**Figure 6G**) networks. In both contexts, the lower
468 affinity C-Raf N64A mutant peaked earlier and had lower overall amplitude than the wildtype C-
469 Raf RBD, and like before, high GAP-networks accentuated these temporal differences.
470 Consistent with this, we found that parameter changes as small as 2-fold could produce subtle
471 shifts in the timing of effector reponses of our kinetic model (Figure 6-figure supplement 2). This
472 shows that new dynamic behaviors are readily realized by mutation of an effector molecule.

473 Taken together, this analysis shows that distinct effector molecules can perceive the same input
474 to a Ras signaling system with different dynamics and amplitudes depending on their affinities
475 and biochemical properties. Consequently, a single step input can be in principle be used
476 encode multiple classes of temporally distinct outputs that peak and decline out of phase with
477 one another, allowing for a sequence of different activities to be organized during signal
478 processing. For example, we were able to produce a three-wave activation response of three
479 distinct effectors in our kinetic model by simply modifying concentrations and off-rates (Figure 6-
480 figure supplement 2). Furthermore, the context of other regulators (e.g. extent of GAP activity in
481 the network) can influence how these different dynamic responses unfold, magnifying temporal
482 distinctions in some cases while restricting the ability of certain effectors to assemble
483 productively at all in other cases. Finally, because even simple point mutations to an effector
484 can dramatically alter its output dynamics, new dynamic patterns are not difficult to produce and
485 can be easily accessed during evolution.

486

487 **Positive feedback ($\text{GTPase}_{\text{ON}} \rightarrow \text{GEF}$) in Ras networks alters signal processing behavior in**
488 **different ways depending on how the feedback mechanism is implemented.**

489 The signaling networks we have examined thus far are solely the product of constitutive
490 enzymatic activities and effector assembly processes unfolding in the simplest possible Ras
491 GTPase signaling circuit. Our analysis found that in high-GAP systems, the “ground state”
492 output for a step-response will transiently overshoot the final steady state. In some instances
493 this behavior could be useful for the cell, for example to create an adaptive response or to
494 produce distinct temporal phases in multiple downstream effector outputs; in other instances
495 this overshoot behavior could prove undesirable, for example if the overshoot provoked a
496 proliferative response to non-proliferative level of input.

497 Many cellular circuits modulate intrinsic behaviors of a signaling system by including additional
498 layers of regulation and feedback control that could alter the signaling properties of the system.
499 To gain insight into how such regulation might alter the ground state signaling behavior of Ras
500 GTPase systems, we examined the effect of introducing two different modes of $\text{GTPase} \rightarrow \text{GEF}$
501 positive feedback (defined as active Ras promoting more activation of Ras) on system signaling
502 behavior.

503

504 *Recruitment-based feedback mechanism ($\text{GTPase}_{\text{ON}} \rightarrow \text{GEF}$ localization) amplifies weak inputs*
505 One common mode of generating positive feedback in signaling is through recruitment. For
506 example, in yeast, the GTPase Cdc42, when activated, recruits its own GEF Cdc24 (via the
507 scaffold Bem1), thus leading to further Cdc42 activation (55). Similar positive feedback GEF
508 recruitment could occur in Ras signaling networks. To explore the effects of recruitment-based
509 positive feedback, we made a synthetic GEF in which we fused the C-Raf RBD effector domain
510 to the RasGRF GEF to produce “RasGRF-RBD”. In this case, the catalytic activity of RasGRF-
511 RBD is always constitutive, but activated Ras will assemble the synthetic GEF on the bead
512 surface to provide a higher effective concentration of GEF and potentially increase the apparent
513 GEF activity (**Figure 7A**). Thus, this feedback mechanism takes an ON GEF molecule and
514 makes it MORE ON as Ras•GTP levels increase. We experimentally measured output
515 responses for this feedback-containing system in 96 system configurations corresponding to 4
516 different input strengths, 4 different GAP concentrations, and 6 different Ras densities (**Figure**
517 **7B**).

518 The inclusion of recruitment-based positive feedback in the system had considerable
519 consequence for both the dynamics and amplitude of the effector output's we observed. For
520 example, in high GEF / high GAP regimes, multiple local maxima in the output dynamics were
521 observed (**Figure 7-figure supplement 1**). Interesting behaviors were also observed for the
522 output amplitudes. For example, because the fluorescent output-effector and the feedback-
523 effector-GEF compete with one another, signaling amplitude did not increase monotonically with
524 increasing INPUT strength: at the highest level of GEF INPUT will examined (2000 nM), signal
525 was substantially lower than at 1000 nM GEF INPUT, and more comparable in amplitude to the
526 200 nM GEF INPUT.

527 How do these differences alter the signaling properties of the system compared to not having
528 this feedback present? Manual inspection of the curves from the system with or without
529 feedback suggested that recruitment-feedback was particularly effective at increasing output in
530 high GAP network contexts. For example, high GEF / low GAP system configurations produced
531 similar responses with or without feedback (**Figure 7C**), but feedback was critical to produce an
532 output from a low GEF / high GAP system configuration (**Figure 7C**). To address this
533 systematically, we calculated a feedback gain for each network configuration we experimentally
534 examined as the ratio of the integrated signal from the feedback system to the non-feedback
535 system. We then interpolated these experimentally determined values for two different Ras
536 density levels to produce phase diagrams showing the impact of feedback on different network
537 configurations (**Figure 7D**).

538 These data imply that this type of feedback mechanism can produce strong effects in certain
539 network configurations but have little to no effect in other configurations. In particular, networks
540 that contained high amounts of basal GAP-activity but only small amounts of input GEF showed
541 the strongest differences in signal. These correspond to regimes in which the amount of GAP
542 activity in the system dominates the small amount of intrinsic catalytic activity of the GEF, but
543 does not overcome the small amount of localized GEF activity arising from the RasGRF-RBD
544 feedback GEF (**Figure 7C**). In contrast, the behaviors of the wildtype and feedback systems
545 were most similar under high GEF, low GAP network configurations. In this regime, the GEF
546 activity from the catalytic domain is sufficient to provide strong activation, and any additional
547 boost in activity for localizing the GEF provides only marginal gains (**Figure 7D**). Thus, this type
548 of feedback mechanism seems most powerful for *amplifying signals arising from weak inputs in*
549 *a high turnover background*.

550

551 Allosteric positive feedback mechanism dampens system overshoot

552 For the second feedback mode, we replaced the RasGRF GEF with SOScat, the catalytic
553 domain from the Son of Sevenless GEF. SOScat has an intrinsic feedback mechanism built in,
554 such that the molecule has very low GEF activity in the absence of Ras•GTP, but Ras•GTP
555 binding to a distal site on SOScat allosterically stimulates GEF activity to very high levels (21,
556 38). Thus, in contrast to the synthetic RasGRF effector fusion (which is always ON), this
557 feedback mechanism takes an OFF GEF molecule and makes it ON in response to Ras•GTP
558 (**Figure 8A**). We experimentally measured output responses for this feedback-containing
559 system in 96 system configurations corresponding to 4 different input strengths, 4 different GAP
560 concentrations, and 6 different Ras densities (**Figure 8B**, normalized responses in **Figure 8-**
561 **figure supplement 1**).

562 These data show a very different effect of the allosteric SOScat feedback on signaling outcomes
563 than was observed for the recruitment-based feedback of the RasGRF-RBD fusion. Unlike with
564 recruitment-based feedback, allosteric-feedback did not provide large gains in output amplitudes
565 in any of the regimes we looked like. However, we did observe that transient overshoot behavior
566 was almost completely absent in the output responses of the SOScat system, even in the
567 highest p120GAP condition we inspected. Indeed, the output dynamics from allosteric-feedback
568 networks appeared much more stable and monotonic than those from RasGRF networks that
569 contained no feedback. These effects were most dramatic in high GAP network contexts in
570 which RasGRF produced a large transient overshoot phase whereas SOScat produced a
571 monotonic approach to the steady state (**Figure 8C**). However, this increased stability was still
572 noticeable even for low GAP high GEF networks in which RasGRF produces a sustained
573 response (**Figure 8C**).

574 These differences in comparison to the RasGRF-RBD positive feedback system can be at least
575 partially attributed to the OFF→ON feedback mechanism of SOScat in the context of a step-
576 input: for a RasGRF GEF step-input, the system experiences a sudden increase in catalytic
577 activity all at once; for SOScat GEF, though, this step-input in protein levels becomes a *ramp-*
578 *input* in terms of protein *activity* because it takes multiple rounds of GEF activity to produce
579 enough Ras•GTP for SOScat to achieve significant activity (**Figure 8D**). Thus, this type of
580 feedback mechanism appears to play less of a role in amplifying weak signals and more of a
581 role in dampening dynamic and transient features that would arise naturally in the step-
582 response without this feedback. For SOScat, which mediates Ras activation in response to
583 growth signals, this overshoot minimization might be a desirable feature that reduces the risk of

584 inappropriate proliferation. This use of biochemical feedback is somewhat analogous to the use
585 of feedback control used in some *electronic* systems to avoid overshoot of the steady-state in
586 response to step-inputs.

587

588 Discussion

589 **One system, many behaviors: a design manual for the diverse signaling behaviors that** 590 **can be constructed with Ras GTPase systems**

591 In this work, we developed a multi-turnover reconstitution of Ras signaling to explore the space
592 of dynamic output behaviors that could be produced by Ras GTPase systems and to
593 characterize how each network component contributes to these behaviors. Using these assays
594 explored how different perturbations such as oncogenic mutation, component levels, inclusion of
595 additional effector molecules, or introducing positive feedback altered the landscape of available
596 outputs.

597 Our experiments imply that, much in the same way that a single genome can encode multiple
598 cell types that are regulated through differential gene expression, a single signaling system like
599 Ras can encode multiple dynamic signal processing behaviors by regulating the concentration
600 and identity of network components. This regulation can be *direct* by acting at the level of gene
601 expression. For example, a simple survey of published p120GAP, Ras, and c-Raf mRNA
602 expression levels across a variety of tissue types reveals a staggering amount of diversity in
603 what types of network configurations are present in different cell types and tissues (**Figure 9A**,
604 **Table S1**). The true diversity in these configurations is likely even greater given the plethora of
605 additional GEFs, GAPs, Ras variants and effectors that cells can deploy. Regulating the
606 concentration of these activities can also be achieved *indirectly* by the differential recruitment of
607 these molecules by the receptors that initiate Ras signaling, which changes their *effective*
608 *concentration* at the plasma membrane. Indeed, many of the catalytic domains that we looked at
609 in this study show regulated interaction dynamics with the plasma membrane in response to
610 extracellular signals (56). Thus, different cells can position their signaling systems at different
611 points in the space of available Ras network configurations and modulate these configurations
612 in response to extracellular cues to provide versatile top-level control of the amplitude and
613 duration of proximal signal processing events (**Figure 9B**).

614 This versatility is not without trade-offs, however. In particular, we observed many different
615 paths in network-space from one signaling processing behavior to another with much higher or
616 sustained amplitude (**Figure 9C**). These paths include classic oncogenic substitutions like G12V
617 in Ras, but can also be realized by increased GEF activity, decreased GAP activity, or inclusion
618 of high-affinity effectors that increase, extend and sustain signaling responses. While some of
619 these perturbations have not been definitively recognized as drivers of cancer, many are
620 associated with other RASopathies in humans, like Noonan syndrome or type 1
621 Neurofibromatosis (7, 57). Thus, the same flexibility that allows Ras systems to realize many
622 different signaling behaviors creates many opportunities for misregulation in response to
623 perturbation.

624 How any particular perturbation distorted signaling output was highly dependent on network
625 configuration. This was most obvious from comparing the effect of Ras G12V perturbation on
626 GAP-free and high-GAP networks (see **Figure 3**), but is also readily apparent from inspection of
627 the structure of our experimental maps between network configuration and signaling outputs
628 (see **Figure 5-figure supplement 2**). Even networks configurations that produced highly similar
629 output behaviors could nonetheless respond divergently to perturbations. These are network
630 configurations along a contour in the phase diagrams and represent neutral paths along which a
631 cell or species can move without immediate consequence to the system. For example, a low
632 signaling output that is maintained by a weak GEF activity alone might also be produced by a
633 higher GEF activity balanced by a high GAP activity. However, these two configurations would
634 respond very differently to substitution with oncogenic alleles of Ras like G12V. This observation
635 demonstrates the limited predictive power of static steady-state measurements of cellular states
636 and highlights the need to obtain *dynamic* data about the pre-steady state and impulse-
637 response behavior of cellular systems using fine-grained time courses or new methods such as
638 optogenetic pathway activation (58).

639 The dependence of a perturbation on network configuration can also afford cells new
640 opportunities that may be positive rather than deleterious. As an example, our analysis of the
641 feedback gain produced by the RasGRF-RBD fusion revealed that some configurations had
642 almost no impact on the system output, while others were highly impacted and produced little to
643 no signal without the presence of feedback (see **Figure 7C-E**). Thus, access to certain regions
644 of this space is not feasible without first acquiring permissive modifications to the feedback
645 architecture of the system. Acquisition of this permissive architecture though, can occur in
646 regions in which there is minimal consequence to the system output. Once this feedback

647 mechanism is present, the space of behaviors available to the system changes and previously
648 non-functional regions of the space can now be accessed.

649 By interrogating the space of available behaviors to a signaling system in an unbiased way as
650 we have in the present work, we learn not only what the behavior of any particular system
651 configuration is, but also how systems respond to *change* and what paths exist to travel to new
652 configurations with new behaviors. For Ras, this space appears rich with dynamic possibilities
653 and sufficient neutral network structure to provide evolution with ample fodder to facilitate the
654 use of Ras for the wide array of diverse signaling roles it plays across different cell types and
655 species, but at the risk of harmful perturbation by diseased alleles or expression states.

656

657 **Building distinct signaling output programs by coupling Ras to multiple effectors.**

658 One striking observation from this work was the importance of effector molecules in determining
659 how a dynamic Ras•GTP signal is interpreted. This is, in fact, a critical aspect of how these
660 particular signaling systems work as activated Ras itself has no *enzymatic* activity towards other
661 molecules, but instead serves only as a platform for the recruitment of many possible competing
662 effector molecules within the cell. Moreover, activated Ras cannot engage more than one
663 effector simultaneously and thus competition between effectors as well as upstream regulators
664 like GAPs contributes to the system's output dynamics.

665 For simple one-effector systems that we studied with the C-Raf RBD effector, the concentration
666 of effector shaped not only the amplitude of the output, but also the dynamics of that output as
667 well (see **Figure 4D**). This is because higher effector concentrations equilibrate against their
668 target faster than lower effector concentrations, resulting in different abilities to capture transient
669 features of the target dynamics. Effector concentration is thus more than a passive "volume"
670 knob that reports on Ras•GTP levels and instead is an active system component that interprets
671 Ras activity to sculpt effector-specific output dynamics owing to its own assembly and
672 disassembly kinetics.

673 The importance of this property of effectors was even more apparent in two-effector Ras
674 signaling systems, in which we found that equivalent amounts of different competing effectors
675 interpreted the same system inputs with markedly different outputs that differed both in
676 amplitudes as well as in duration and dynamics (see **Figure 6**). These systems showed a
677 variety of interesting multi-effector programs, such as one effector exhibiting a transient

678 response while another was sustained, one effector responding while another did not at all, or
679 two transient responses that peaked and declined with different timing and duration. Moreover,
680 we found that different dynamic behaviors could readily be produced by introducing point
681 mutations in an effector that altered affinity for activated Ras. These observations stress the
682 important roles that both kinetic and thermodynamic aspects of effector assembly and
683 competition play in shaping how an individual effector interprets dynamic Ras•GTP levels in the
684 context of the rest of the network.

685 An interesting consequence of these different effector behaviors and dynamics is that it can
686 naturally result in the temporal partitioning of distinct activities during a signaling response. This
687 can allow some effector outputs to be restricted to early phases of signaling, only to decline and
688 be displaced by other more dominant effectors at later stages. These observations extend
689 recent observations of hierarchies of binding by different effectors to Ras under equilibrium
690 conditions with non-hydrolyzable analogs (45). Thus, the differential perception of Ras•GTP
691 signals by distinct effectors may not be a flaw in the method by which cells make
692 measurements, but a useful feature by which cells can use a single upstream signaling
693 molecule like Ras to dictate a complex temporal program of multiple downstream outputs.

694

695 **Additional signal processing mechanisms operate in the context of complex Ras effector
696 binding dynamics.**

697 Binding to activated Ras is only the first step in signal propagation for many effectors. For
698 example, binding of Raf kinases we used in this study to Ras primarily serves to deliver the
699 kinase to the plasma membrane where its interaction with lipids (59), other Raf kinases (60),
700 scaffolds (61, 62) and other macromolecules alters its kinase activity and thus how it sends out
701 signals downstream (REF). In fact, Raf can even activate downstream signaling in the absence
702 of Ras by artificial membrane recruitment (37, 63). However, this only further emphasizes the
703 importance of effector binding *dynamics* in the context of cellular signal processing, as binding
704 to Ras is a physiological prerequisite for these other mechanisms to take place. Moreover,
705 different Ras effectors such as PI3 Kinase or Ral-GDS will have their own molecule-specific
706 layers of regulation that take place upon interaction with Ras at the plasma membrane. These
707 processes will be influenced by the underlying effector-binding dynamics in different ways
708 depending on the kinetics of these downstream steps. Our work demonstrates that cells have

709 simple systems for modulating and controlling these fundamental binding dynamics and further
710 indicates that known control mechanisms should be analyzed in this complex dynamic context.

711 Another layer of dynamic and regulatory complexity is also likely to arise as more classes of
712 Ras GTPases are included in the signaling networks. Indeed, our present study has only
713 investigated effector interaction with H-Ras, but there exist many additional Ras isoforms such
714 as K-Ras and N-Ras, K4A-Ras, and K4B-Ras that may engage these effectors in different ways
715 to produce different dynamics. Additionally, there exist related GTPases such as Rap which can
716 serve as platform for Ras effectors but that do not necessarily promote signal propagation (64,
717 65). Understanding how the underlying distribution of GTPase isoforms dictates signal
718 processing behavior is another critical component of cellular signaling and we hope to extend
719 our *in vitro* system to explore these fundamental questions in the future.

720

721 **Systems-level reconstitution as tool to probe the mechanism of biochemical signal
722 processing networks.**

723 The network level biochemical approach to interrogating signaling systems we employed in this
724 study occupies a relatively underexplored area in our understanding of cellular decision making
725 systems, but is similar to approaches used to understand dynamic *mechanical* systems in cells
726 like microtubules. Indeed, because additional complexities can emerge when multiple
727 energetically driven processes are coupled together to promote the dynamic assembly and
728 disassembly of competing effectors, exploring how these systems behave *in vitro* under different
729 configurations sheds new light on the phenomenology of how biochemical signaling devices
730 function and respond to perturbation.

731 The ability to prepare non-equilibrium steady states in which Ras is actively cycling between ON
732 and OFF states may also prove useful in developing new strategies to ameliorate erroneous
733 signaling associated with diseased states. For example, the fact that we could reconstitute
734 radically different signaling behaviors for wildtype and G12V Ras under high GAP conditions is
735 consistent with the notion that wildtype Ras ordinarily cycles quickly but G12V does not. This
736 difference in the *lifetime* of a Ras•GTP molecule compared to RasG12V•GTP could potentially
737 serve as an additional *dynamic* selectivity handle for small molecules in which we want to only
738 target the oncogenic form of Ras. The assays we developed are well suited to compare how
739 small molecules differentially impact signaling through these different forms of Ras side by side
740 under active energy-consuming conditions.

741 More generally, the simplicity of the approach we present here paves the way for further studies
742 on other types of non-equilibrium signaling systems that center around the assembly of
743 molecules from the cytoplasm on a surface such as the other members of the Ras superfamily
744 like Rho, Rac, Cdc42 and Rab GTPases, as well as other completely different multi-turnover
745 signaling systems like receptor tyrosine kinases or lipid kinases. Some aspects of the H-Ras
746 system may be shared with these systems, while other aspects may be different owing to
747 idiosyncratic features of a particular system of molecules. These systems could also be
748 extended in other ways as well to explore how other biophysical constraints impact these
749 signaling processes. Our reconstitutions could, for example, be extended to lipid-coated beads
750 to explore how membrane fluidity or lipid identity shape effector outputs. Multi-currency
751 networks that include multiple Ras isoforms or contain more than one type of GTPase could
752 also be examined to look at higher-order networks and cascades. Only by building these
753 systems, turning them on and watching them run can we begin to understand how they actually
754 perform and operate in different signaling regimes.

755

756 Materials and methods

757 Protein Purification

758 *Purification, labeling, and nucleotide loading of GTPases*

759 Full-length H-Ras, H-Ras(G12V), H-Ras (G12C), and H-Ras(Q61L) were expressed as N-
760 terminal SNAPtag-(GAGS)_{2x}-MBP C-terminal DoubleHisTag (10xHis-(GAGS)_{3x}-6xHis) fusion
761 proteins using custom expression plasmids (see plasmids table). The SNAP-tag facilitated
762 labeling with high-performance inorganic dyes for imaging, and the DoubleHisTag on the C-
763 terminus allowed Ni-NTA supports to be loaded stably ($t_{1/2} > 24$ hours) with GTPase in a
764 configuration resembling the native C-terminal attachment mode.

765 To express protein, BL21(T1R) *E. coli* cells were grown to an OD of 0.4 from a fresh
766 transformation, chilled to 18°C, induced with 0.8 mM IPTG, and allowed to express overnight.
767 The proteins were purified by Ni-NTA affinity chromatography following the manufacturer's
768 instructions, but were eluted in the presence of 1M Imidazole to facilitate elution of the
769 DoubleHisTag. Proteins were subsequently purified by amylose affinity chromatography per the
770 manufacturer's guidelines. The protein was then concentrated to ~0.5 mL and purified by gel-
771 filtration chromatography on a Superdex S200 10/300 equilibrated in Nucleotide Exchange

772 Buffer (5 mM EDTA, 20 mM Tris, 150 mM NaCl, pH 8.0) to remove any bound nucleotide from
773 the GTPase.

774 Labeling of the SNAPtag on the GTPases was performed per the manufacturer's instructions.
775 Briefly, samples were buffer-exchanged into a labeling buffer (150 mM NaCl, 25 mM Tris, pH
776 7.5) using a zebra desalting column. Following twenty minute incubation with 5 mM DTT at 37°,
777 SNAP-Cell 430 substrate was added at a 1.1:1 dye:protein molar ratio and incubated for 1 hour
778 at 37°C or overnight at 4°C. Unlabeled dye was removed by passing the sample through 4
779 zebra desalting columns.

780 The labeled GTPases were loaded with nucleotide using established protocols (27). Briefly,
781 GTPases were exchanged into Nucleotide Exchange Buffer using a zebra desalting column and
782 incubated with a 20-fold molar excess of nucleotide (typically GDP) for thirty minutes at room
783 temperature. The loading reaction was quenched by the addition of MgCl₂ to 10 mM. Unloaded
784 nucleotide was removed by passing the sample through 4 zebra desalting columns. Samples
785 were finally exchanged into GTPase storage buffer (20 mM Tris, 50 mM NaCl, 10 mM MgCl₂,
786 5% glycerol, pH 7.5), concentrated to ~100 μM, aliquotted, flash-frozen, and stored at -80°C.

787

788 *Purification and labeling of effectors.*

789 The RBD effector domains of A-Raf, B-Raf, C-Raf and any associated mutants were expressed
790 as N-terminal SNAPtag-(GAGS)_{2x}-MBP C-terminal Strep-II tag fusions. The SNAP-tag facilitated
791 labeling with high-performance inorganic dyes for imaging, and the Strep-II tag provided a
792 handle for affinity chromatography that did not interact with Ni-NTA supports.

793 To express protein BL21(T1R) *E. coli* cells were grown to an OD of 0.8 from a fresh
794 transformation, chilled to 18°C, induced with 0.8 mM IPTG, and allowed to express overnight.
795 The proteins were purified by Streptactin affinity chromatography and then amylose affinity
796 chromatography, per the manufacturer's instructions. Proteins were concentrated to ~1 mL and
797 further purified by gel-filtration chromatography on a Superdex S75 16/60 equilibrated in
798 standard protein buffer (150 mM NaCl, 25 mM Tris pH 7.5).

799 Labeling of the SNAPtag on the effectors was performed per the manufacturer's instructions.
800 Briefly, samples were incubated with 5 mM DTT at 37°C for twenty minutes. SNAP-Surface 488
801 or SNAP-Surface 549 were added at a 1.1:1 dye:protein molar ratio and incubated for 1 hour at
802 37 or overnight at 4 degrees. Unlabeled dye was removed by passing the sample through 4

803 zebra desalting columns. Samples were concentrated to 100 uM, exchanged into storage buffer
804 (150 mM NaCl, 25 mM Tris pH 7.5, 5% glycerol), aliquotted, flash frozen and stored at -80°C.

805

806 *Purification of GEFs, GAPs, and synthetic effector-GEF fusions.*

807 The catalytic domains of RasGRF, p120GAP, NF1-GAP, SOS and RBD-RasGRF were
808 expressed as N-terminal MBP C-terminal Strep-II tag fusions. The Strep-II tag provided a
809 handle for affinity chromatography that did not interact with Ni-NTA supports.

810 To express protein BL21(T1R) *E. coli* cells were grown to an OD of 0.4 from a fresh
811 transformation, chilled to 18°C, induced with 0.8 mM IPTG, and allowed to express overnight.
812 The proteins were purified by Streptactin affinity chromatography and then amylose affinity
813 chromatography, per the manufacturer's instructions. Proteins were concentrated to ~0.5 mL
814 and purified by gel-filtration chromatography on a Superdex S200 10/300 equilibrated in
815 standard protein storage buffer (150 mM NaCl, 25 mM Tris pH 7.5, 5% glycerol). Proteins were
816 concentrated, aliquotted, flash frozen, and stored at -80°C

817

818 **In Vitro Signal Processing Assays**

819 *Preparation of GTPase loaded beads*

820 50 uL of NiSepharose High Performance beads (GE Healthcare) were washed twice with 1 mL
821 water, twice with GTPase assay buffer (GAB: 20 mM Tris, 50 mM NaCl, 10 mM MgCl₂, 30 mM
822 Imidazole), and resuspended in a final volume of 1 mL GAB. To load beads, 7.5 uL of this bead
823 slurry was mixed with 7.5 uL of GTPase in a PCR tube and incubated on ice for 1 hour with
824 occasional flicking. The amount of GTPase used to load the beads depending on the desired
825 density for the specific experiments being performed downstream, but a typical bead-loading
826 used 7.5 μL of 30 μM GTPase and typically resulted in Ras densities crudely estimated at 2500
827 molecules × μm⁻² (see calculation below). Following incubation, the beads were spun in a table-
828 top minifuge, the supernatant removed, and washed 3 times with GAB. The washed beads were
829 resuspended in ~100 μL GAB, transferred to an Eppendorf tube, shielded from light, and stored
830 on ice. The exact amount of final GAB the beads were in was adjusted for any particular
831 experiment such that 2 μL of bead slurry contained roughly 25-100 total beads when placed in a
832 384 well microscopy plate.

833

834 *Preparation of signal processing reactions and data collection*

835 Signal processing reactions were set up in two stages. First, a “bead-mix” was prepared that
836 contained fluorescent effector at the desired concentration (typically 50 nM) and beads in GAB.
837 It should be noted that the inclusion of 20 mM Imidazole was critical for eliminating non-specific
838 background effector staining on the bead surface and improved reproducibility dramatically. 20
839 µL of this bead mix was dispensed into the wells of a 384-well Costar microscopy plate. Second,
840 an “initiation-mix” was prepared that contained fluorescent effector at the desired concentration,
841 5 mM GTP (or other nucleotide if used) and GEFs and GAPs at the desired concentration, all in
842 GAB. 10 ul of this reaction mix was gently added to the 20 µl bead mix in the 384-well plate to
843 initiate reaction. The large volume of the initiation mix was critical for getting sufficient mixing
844 without the need to pipette up and down and disrupt the beads and improved reproducibility.
845 Once signal processing reactions were initiated, they wells were sealed with PCR plate sealant
846 to prevent evaporation.

847 All data was collected on a Nikon Eclipse TI inverted microscope equipped with a Yokogawa
848 CSU-X1 spinning disk confocal using a 20x PlanAPO 0.75 NA objective and an electron
849 microscopy charge-coupled device (EM-CCD) camera (Andor). Depending on the experiment,
850 405 nm, 488 nm, and/or 561 nm wavelength laser light (LMM5, Spectral applied Research)
851 were used for excitation.

852 For typical experiments, 5-10 x-y positions within a given well were used to collect signal
853 processing behaviors from 20-100 individual beads. Timepoints varied depending on the
854 experiment, but for typical large matrix experiments of 24-60 different GEF/GAP/effector
855 conditions, we typically imaged every 15 minutes for 6-12 hours. MicroManager software was
856 used to design the imaging protocols and collect the actual data.

857

858 **Image Analysis, Data Processing and Statistics**

859 A combination of standard and custom ImageJ macros were used to prepare the primary image
860 data for further analysis. First, drift in the stage was corrected using a macro based around the
861 MultiStackReg plugin. Two or three color multi-tiff timecourses were split into separate
862 channels. Matrix transformations to register timecourses were obtained using the constant
863 GTPase fluorescence on every bead from the blue channel. These matrices were then used to

864 register the timecourses of the red or green channels. The three channels were then
865 recombined to produce the properly registered multi-tiff used for analysis of the beads. The
866 ImageJ macro code was tweaked depending on the particular experiment, but a representative
867 example of the code is shown below:

```
868     matrixxpath= "C:\\\\Users\\\\scoyl_000\\\\Google Drive\\\\MICROSCOPY\\\\150403\\\\matrix\\\\";  
869     inputpath = "C:\\\\Users\\\\scoyl_000\\\\Google Drive\\\\MICROSCOPY\\\\150403\\\\raw\\\\";  
870     outputpath = "C:\\\\Users\\\\scoyl_000\\\\Google Drive\\\\MICROSCOPY\\\\150403\\\\processed\\\\";  
871  
872  
873     function scott_register(input,output,filename) {  
874         open(input+filename);  
875         run("Split Channels");  
876         run("MultiStackReg", "stack_1=[C3-" + filename + "] action_1=Align  
877 file_1=[\"+matrixxpath+\"matrix.txt] stack_2=None action_2=Ignore file_2=[] transformation=[Rigid Body]  
878 save");  
879         run("MultiStackReg", "stack_1=[C1-" + filename + "] action_1=[Load Transformation File]  
880 file_1=[\"+matrixxpath+\"matrix.txt] stack_2=None action_2=Ignore file_2=[] transformation=[Rigid  
881 Body]");  
882         run("MultiStackReg", "stack_1=[C2-" + filename + "] action_1=[Load Transformation File]  
883 file_1=[\"+matrixxpath+\"matrix.txt] stack_2=None action_2=Ignore file_2=[] transformation=[Rigid  
884 Body]");  
885         run("Merge Channels...", "c1=C1-" + filename + " c2=C2-" + filename + " c3=C3-" + filename + "  
886 create");  
887     }  
888  
889     list = getFileList(inputpath);  
890     for (i = 0; i < list.length; i++)  
891         scott_register(inputpath, outputpath, list[i]);  
892
```

893 We then corrected for uneven sample illumination or background artifacts using a rolling ball
894 background subtraction of 50 pixels. These processed images were subsequently used to
895 analyze the signaling behavior of each bead.

896 To analyze the images, beads were either identified and stored as regions-of-interest (ROIs)
897 automatically from the GTPase fluorescent signal on beads using a custom macro that makes
898 use of ImageJ's "find particles" function, or in the case of experiments with beads that
899 deliberately contain differing levels of Ras density, beads were identified and stored as ROIs by
900 hand. The particular parameters of the automated bead finding varied depending on the
901 particular experiment, but a representative ImageJ macro is shown below:

902

```
903     inputpath = "C:\\\\Users\\\\scoyl_000\\\\Google Drive\\\\MICROSCOPY\\\\150403\\\\processed\\\\";  
904     outputpath = "C:\\\\Users\\\\scoyl_000\\\\Google Drive\\\\MICROSCOPY\\\\150403\\\\beads\\\\";  
905
```

```

906     function scott_findbeads(input,output,filename) {
907
908         open(input+filename);
909         run("Split Channels");
910
911         selectWindow("C3-" + filename);
912         run("Smooth", "stack");
913
914         //set threshold and find particles
915         Stack.setPosition(1, 18,1);
916         setSlice(20);
917         setThreshold(3744, 23285);
918         run("Analyze Particles...", "size=400-15000 circularity=0.60-1.00 display exclude clear
919         include add slice");
920
921         //close any and all open windows
922         close();
923         close();
924         close();
925
926
927         //reopen original file
928         open(input+filename);
929
930         //transfer ROIs to overlay and save
931         run("From ROI Manager");
932         saveAs("Tiff", output+filename);
933
934         //clear manager
935         roiManager("Delete");
936         close();
937     }
938
939     list = getFileList(inputpath);
940     for (i = 0; i < list.length; i++)
941         scott_findbeads(inputpath, outputpath, list[i]);
942

```

943 Once beads were identified and stored as ROIs, a variety of measurements were made for each
944 bead using a custom macro. We measured the average total Ras fluorescence in the ROI, and
945 the average fluorescent effector signal in the ROI at every timepoint in the experiment. We also
946 measured the area and perimeter of the bead. As with other macros, the exact details of the
947 code varied depending on the number of effectors we were simultaneously examining or other
948 aspects of the setup, but a representative ImageJ macro is shown below:

```

949
950     inputpath = "C:\\\\Users\\\\scoyl_000\\\\Google Drive\\\\MICROSCOPY\\\\150318\\\\one_shot_processed\\\\";
951     outputpath = "C:\\\\Users\\\\scoyl_000\\\\Google Drive\\\\MICROSCOPY\\\\150318\\\\one_shot_data\\\\";
952
953     setBatchMode(true);
954     list = getFileList(inputpath);

```

```

955     for (i = 0; i < list.length; i++)
956         crunchimage(inputpath, outputpath, list[i]);
957     setBatchMode(false);
958
959     //The Functions that are used in the macro are below
960
961     function crunchimage(input,output,filename) {
962
963         //open the image
964         open(input+filename);
965
966         //clear log file and reulsts table
967         run("Clear Results");
968         print("\\\\Clear");
969
970         //import ROIs from overlay
971         run("To ROI Manager");
972
973         //count ROIs
974         count=roiManager("count");
975
976         //record Ras AMPS and RBD timecourse for each ROI
977         for(i=0;i<count;i++){
978
979             // first record the AMP for the Ras field;
980
981             recordAMP(i);
982
983             // next calculate the time series for the data
984
985             recordTimecourse(i);
986
987             // print newline marker
988
989             print("!");
990         }
991
992         selectWindow("Log");
993         saveAs("Text", output+filename);
994         close();
995
996
997     }
998
999     function recordAMP(index) {
1000         //function that reports area, mean intensity, and perimieter
1001         // of an ROI used to get everything EXCEPT the timecourse data
1002
1003         run("Clear Results");
1004         roiManager("Select",index);
1005
1006         // select channel 2 and select the midpoint of hte stack
1007
1008         Stack.setPosition(2, 18,18);

```

```

1009
1010      // make measurements
1011
1012      run("Measure");
1013      BeadArea=getResult("Area",0);
1014      BeadMean=getResult("Mean",0);
1015      BeadPerim=getResult("Perim.",0);
1016      print(BeadArea+","+BeadMean+","+BeadPerim+",");
1017
1018  }
1019
1020  function recordTimecourse(index){
1021      run("Clear Results");
1022      roiManager("Select",index);
1023      sliceCount=nSlices()/2;
1024      // print(sliceCount);
1025
1026      for(k=0;k<sliceCount;k++){
1027          Stack.setPosition(1, 18,k+1);
1028          run("Measure");
1029          timepointK=getResult("Mean",k);
1030          print(timepointK+",");
1031      }
1032
1033
1034  }
1035
1036

```

1037 The output of this macro is a file that contains a list of every single bead trace in the multi-tiff
 1038 image. Each trace begins with the area measurement of the bead, the mean total Ras intensity
 1039 of the bead, and the perimeter measurement of the bead, followed by the effector measurement
 1040 of the bead at every timepoint. Each measurement ends with a "," and is on a newline. At the
 1041 end of each bead trace, a stop marker "!" is printed. These data are then transformed by GREP
 1042 and shell script into a CSV where each line contains all the relevant information about each
 1043 single bead's signaling trace. These data can then be loaded into either Matlab or Excel for
 1044 further analysis.

1045 Once in Excel, data were typically further analyzed as follows: (i) intensity measurements were
 1046 normalized to perimeter instead of area, (ii) the time-series data for a given bead was
 1047 normalized such that the time-zero effector measurement was zero, (iii) single bead traces were
 1048 binned based on total GTPase levels to obtain statistics on the signaling behavior. Beads were
 1049 assigned to the nearest of the 6 Ras density beads: 150 molecules / um², 300 molecules / um²,
 1050 600 molecules / um², 1200 molecules / um², 2500 molecules / um², 10,000 molecules / um².
 1051 The individual bead traces within a given bin were then averaged together to produce an

1052 average response for the associated density bin and network configuration. Each trace was
1053 typically the average of 15-80 beads from the combination of two independent experiments. The
1054 standard error of the mean for a given trace was typically < 15%.

1055

1056 *Estimation of Ras Density*

1057 We estimated the approximate Ras density of a bead in molecules $\times \mu\text{m}^{-2}$ in the following
1058 manner. First we determined the correspondence between the concentration of labeled Ras and
1059 its fluorescence intensity by imaging serial dilutions of known concentrations of SNAP-Cell 430
1060 labeled Ras in solution. From this we could associate a particular fluorescence intensity with a
1061 three-dimensional concentration in μM . For our imaging conditions, this relationships was:

1062

1063 $\text{Concentration } (\mu\text{M}) = 4.287 \text{ } (\mu\text{M} \times \text{AU}^{-1}) \times \text{Intensity } (\text{AU})$

1064

1065 For any individual bead then, there is some maximum fluorescence intensity on the bead
1066 surface that we can associate with an apparent three-dimensional concentration. This apparent-
1067 three dimensional concentration can be used to estimate an inferred two-dimensional density by
1068 assuming that the apparent three-dimensional concentration is a consequence of molecules
1069 within some two-dimensional area exploring three-dimensional space as constrained by some
1070 confinement length h (66, 67). We use an h obtained from previously published work on EGFR
1071 kinases tethered by His-tags to a DGS-NTA(Ni) charged vesicle surface, which assumed a
1072 radius of confinement of 55 nm (66). Given that 1 μM corresponds to ~ 602 molecules / μm^3 , this
1073 enabled us to convert between three-dimensional and two-dimensional concentrations using the
1074 relation:

1075 $1 \text{ } \mu\text{M} \times (602 \text{ (molecules } \times \mu\text{m}^{-3}) \times \mu\text{M}^{-1}) * 0.055 \text{ } \mu\text{m} = 33.1 \text{ molecules } \mu\text{m}^{-2}$

1076 $\Rightarrow \text{2-D Concentration (molecules } \times \mu\text{m}^{-2}) =$

1077 $3\text{-D concentration } (\mu\text{M}) * 33.1 \text{ ((molecules } \times \mu\text{m}^2) \times \mu\text{M}^{-1})$

1078 We stress that this is only an *estimate* of the Ras density and should not be taken as a highly
1079 accurate assessment of the Ras density. Nonetheless, it provides a crude estimation that
1080 indicates that our experiments are not operating in a highly non-physiologic regime. Importantly,

1081 for our analysis the exact number of Ras molecules on the bead surface is not critical. Indeed,
1082 the relative abundances of Ras on different beads is more important as it enables us to
1083 compare behaviors between beads as Ras densities change.

1084

1085 **Kinetic modeling and simulation**

1086 Kintek Student Explorer (68) was used to simulate the dynamic behavior of a variety of models
1087 for GTPase activation. Time was modeled in seconds and concentrations in nM. Rate constants
1088 for association and dissociation of molecules from the GTPase were based on published
1089 Biacore measurements (53), and catalytic rate constants for GEF and GAP activities were
1090 based published solution measurements (26, 38). GEF was not modeled explicitly but rather
1091 directly incorporated in the rate constant for nucleotide release. Each simulation was allowed to
1092 run for 42000 seconds (~700 min).

1093 Three models were initially explored. The first model was a 2-state GTPase model that did not
1094 account for competition between GAP and effector. This was modeled in Kintek using the
1095 following equations and parameters:

	k-	k+
G + T = GT	1	0
GT = GD	0.0001*[GAP]	0
GD = G + D	0.05	0
GT + EFF = GT_EFF	0.0001	0.001
GT_EFF = GD + EFF	0.0001	0

1096

1097 The second model was a 2-state GTPase model that explicitly modeled competition between
1098 GAP and effector. This was modeled in Kintek using the following equations and (physiological)
1099 parameters:

	k+	k-
G + T = GT	1	0
GT = GD	0.0001	0
GD = G + D	0.00505	0
GT + EFF = GT_EFF	0.0001	0.001
GT_EFF = GD + EFF	0.0001	0
GT + GAP = GT_GAP	0.0001	0.01
GT_GAP = GD + GAP	1	0

1100

1101 The third model was a 3-state GTPase model that included an additional post-hydrolysis
1102 GTPase state (GI) which was refractory to GEF activation. This state converts to the GDP form
1103 on a slow timescale. This was modeled in Kintek as:

	k+	k-
G + T = GT	1	0
GT = GI	0.0001	0
GI = GD	0.0001	0
GD = G + D	0.005	0
GT + EFF = GT_EFF	0.0001	0.001
GT_EFF = GI + EFF	0.0001	0
GT + GAP = GT_GAP	0.0001	0.01
GT_GAP = GI + GAP	1	0

1104

1105 The third model was the best at explaining the transient behaviors of the system that we
1106 observed as well as the differences between WT and G12V Ras, and thus was used as the
1107 basis of all subsequent modeling and simulations. For any given simulation in the text, the initial
1108 conditions and any changes to associated rate-constants are indicated in the figure legend.

1109

1110 **Comparison of Network Configurations Across Cell and Tissue Types.**

1111 Relative log-transformed expression levels for p120GAP, C-Raf, and H-Ras across a variety of
1112 cell-types and tissue-types were obtained from data contained within the Genevestigator
1113 software package (see data in **Table S1**). The three-dimensional phenotypes associated with
1114 each cell or tissue type was plotted as a 3D scatterplot using Matlab.

1115

1116 **ACKNOWLEDGMENTS**

1117 S.M.C. was supported by a National Science Foundation Graduate Research Fellowship. This
1118 work was supported by NIH grants RO1 GM55040, PN2 EY016546, P50 6M081879 (W.A.L.),
1119 and the Howard Hughes Medical Institute (W.A.L.). We thank T. Anooki, L. Bugaj, R. Gordley,
1120 R.S. Isaac, A. Mitchell, G. O' Donoghue, K. Roybal, M. Thomson, J. Walter, and A. Weeks for
1121 helpful discussions.

1122

1123 **References**

- 1124 1. F. Chang *et al.*, Regulation of cell cycle progression and apoptosis by the
1125 Ras/Raf/MEK/ERK pathway (Review). *Int. J. Oncol.* **22**, 469–480 (2003).
- 1126 2. A. Sjölander, K. Yamamoto, B. E. Huber, E. G. Lapetina, Association of p21ras with
1127 phosphatidylinositol 3-kinase. *Proc. Natl. Acad. Sci. U. S. A.* **88**, 7908–7912 (1991).
- 1128 3. F. Hofer, S. Fields, C. Schneider, G. S. Martin, Activated Ras interacts with the Ral
1129 guanine nucleotide dissociation stimulator. *Proc. Natl. Acad. Sci. U. S. A.* **91**, 11089–
1130 11093 (1994).
- 1131 4. A. B. Vojtek, C. J. Der, Increasing Complexity of the Ras Signaling Pathway. *J. Biol. Chem.*
1132 **273**, 19925–19928 (1998).
- 1133 5. H. R. Bourne, D. A. Sanders, F. McCormick, The GTPase superfamily: a conserved switch
1134 for diverse cell functions. *Nature*. **348**, 125–132 (1990).
- 1135 6. J. L. Bos, ras oncogenes in human cancer: a review. *Cancer Res.* **49**, 4682–4689 (1989).
- 1136 7. S. Schubbert, K. Shannon, G. Bollag, Hyperactive Ras in developmental disorders and
1137 cancer. *Nat. Rev. Cancer*. **7**, 295–308 (2007).
- 1138 8. U. Krengel *et al.*, Three-dimensional structures of H-ras p21 mutants: Molecular basis for
1139 their inability to function as signal switch molecules. *Cell*. **62**, 539–548 (1990).
- 1140 9. M. V. Milburn *et al.*, Molecular switch for signal transduction: structural differences between
1141 active and inactive forms of protooncogenic ras proteins. *Science*. **247**, 939–945 (1990).
- 1142 10. N. Nassar *et al.*, The 2.2 Å crystal structure of the Ras-binding domain of the
1143 serine/threonine kinase c-Raf1 in complex with Rap1A and a GTP analogue. *Nature*. **375**,
1144 554–560 (1995).
- 1145 11. C. Herrmann, Ras–effector interactions: after one decade. *Curr. Opin. Struct. Biol.* **13**,
1146 122–129 (2003).
- 1147 12. S. E. Neal, J. F. Eccleston, A. Hall, M. R. Webb, Kinetic analysis of the hydrolysis of GTP
1148 by p21N-ras. The basal GTPase mechanism. *J. Biol. Chem.* **263**, 19718–19722 (1988).
- 1149 13. J. B. Gibbs, I. S. Sigal, M. Poe, E. M. Scolnick, Intrinsic GTPase activity distinguishes
1150 normal and oncogenic ras p21 molecules. *Proc. Natl. Acad. Sci.* **81**, 5704–5708 (1984).
- 1151 14. J. P. McGrath, D. J. Capon, D. V. Goeddel, A. D. Levinson, Comparative biochemical
1152 properties of normal and activated human ras p21 protein. *Nature*. **310**, 644–649 (1984).
- 1153 15. M. S. Boguski, F. McCormick, Proteins regulating Ras and its relatives. *Nature*. **366**, 643–
1154 654 (1993).
- 1155 16. M. Trahey, F. McCormick, A cytoplasmic protein stimulates normal N-ras p21 GTPase, but
1156 does not affect oncogenic mutants. *Science*. **238**, 542–545 (1987).

- 1157 17. J. L. Bos, H. Rehmann, A. Wittinghofer, GEFs and GAPs: Critical Elements in the Control
1158 of Small G Proteins. *Cell*. **129**, 865–877 (2007).
- 1159 18. F. McCormick, G. A. Martin, R. Clark, G. Bollag, P. Polakis, Regulation of ras p21 by
1160 GTPase Activating Proteins. *Cold Spring Harb. Symp. Quant. Biol.* **56**, 237–241 (1991).
- 1161 19. C. Lenzen, R. H. Cool, H. Prinz, J. Kuhlmann, A. Wittinghofer, Kinetic Analysis by
1162 Fluorescence of the Interaction between Ras and the Catalytic Domain of the Guanine
1163 Nucleotide Exchange Factor Cdc25Mm. *Biochemistry (Mosc.)*. **37**, 7420–7430 (1998).
- 1164 20. H. Sondermann *et al.*, Structural Analysis of Autoinhibition in the Ras Activator Son of
1165 Sevenless. *Cell*. **119**, 393–405 (2004).
- 1166 21. S. M. Margarit *et al.*, Structural Evidence for Feedback Activation by Ras·GTP of the Ras-
1167 Specific Nucleotide Exchange Factor SOS. *Cell*. **112**, 685–695 (2003).
- 1168 22. J. S. Iwig *et al.*, Structural analysis of autoinhibition in the Ras-specific exchange factor
1169 RasGRP1. *eLife*. **2**, e00813 (2013).
- 1170 23. K. Scheffzek *et al.*, The Ras-RasGAP Complex: Structural Basis for GTPase Activation
1171 and Its Loss in Oncogenic Ras Mutants. *Science*. **277**, 333–339 (1997).
- 1172 24. P. A. Boriack-Sjodin, S. M. Margarit, D. Bar-Sagi, J. Kuriyan, The structural basis of the
1173 activation of Ras by Sos. *Nature*. **394**, 337–343 (1998).
- 1174 25. L. Feng *et al.*, PKA phosphorylation and 14-3-3 interaction regulate the function of
1175 neurofibromatosis type I tumor suppressor, neurofibromin. *FEBS Lett.* **557**, 275–282
1176 (2004).
- 1177 26. G. Bollag, F. McCormick, Differential regulation of rasGAP and neurofibromatosis gene
1178 product activities. *Nature*. **351**, 576–579 (1991).
- 1179 27. A. Eberth, M. R. Ahmadian, in *Current Protocols in Cell Biology* (John Wiley & Sons, Inc.,
1180 2001; <http://onlinelibrary.wiley.com/doi/10.1002/0471143030.cb1409s43/abstract>).
- 1181 28. M. Geyer *et al.*, Conformational Transitions in p21ras and in Its Complexes with the
1182 Effector Protein Raf-RBD and the GTPase Activating Protein GAP. *Biochemistry (Mosc.)*.
1183 **35**, 10308–10320 (1996).
- 1184 29. C. Herrmann, G. Horn, M. Spaargaren, A. Wittinghofer, Differential Interaction of the Ras
1185 Family GTP-binding Proteins H-Ras, Rap1A, and R-Ras with the Putative Effector
1186 Molecules Raf Kinase and Ral-Guanine Nucleotide Exchange Factor. *J. Biol. Chem.* **271**,
1187 6794–6800 (1996).
- 1188 30. J. R. Sydor, M. Engelhard, A. Wittinghofer, R. S. Goody, C. Herrmann, Transient Kinetic
1189 Studies on the Interaction of Ras and the Ras-Binding Domain of c-Raf-1 Reveal Rapid
1190 Equilibration of the Complex. *Biochemistry (Mosc.)*. **37**, 14292–14299 (1998).
- 1191 31. I. Rubio *et al.*, TCR-Induced Activation of Ras Proceeds at the Plasma Membrane and
1192 Requires Palmitoylation of N-Ras. *J. Immunol.* **185**, 3536–3543 (2010).

- 1193 32. H. Murakoshi *et al.*, Single-molecule imaging analysis of Ras activation in living cells. *Proc.
1194 Natl. Acad. Sci. U. S. A.* **101**, 7317–7322 (2004).
- 1195 33. X. Nan *et al.*, Ras-GTP dimers activate the Mitogen-Activated Protein Kinase (MAPK)
1196 pathway. *Proc. Natl. Acad. Sci.* **112**, 7996–8001 (2015).
- 1197 34. T. Tian *et al.*, Plasma membrane nanoswitches generate high-fidelity Ras signal
1198 transduction. *Nat. Cell Biol.* **9**, 905–914 (2007).
- 1199 35. J. R. Silvius, P. Bhagatji, R. Leventis, D. Terrone, K-ras4B and prenylated proteins lacking
1200 “second signals” associate dynamically with cellular membranes. *Mol. Biol. Cell.* **17**, 192–
1201 202 (2006).
- 1202 36. T. Jelinek, P. Dent, T. W. Sturgill, M. J. Weber, Ras-induced activation of Raf-1 is
1203 dependent on tyrosine phosphorylation. *Mol. Cell. Biol.* **16**, 1027–1034 (1996).
- 1204 37. D. Stokoe, S. G. Macdonald, K. Cadwallader, M. Symons, J. F. Hancock, Activation of Raf
1205 as a result of recruitment to the plasma membrane. *Science* **264**, 1463–1467 (1994).
- 1206 38. T. S. Freedman *et al.*, A Ras-induced conformational switch in the Ras activator Son of
1207 sevenless. *Proc. Natl. Acad. Sci.* **103**, 16692–16697 (2006).
- 1208 39. C. Block, R. Janknecht, C. Herrmann, N. Nassar, A. Wittinghofer, Quantitative structure-
1209 activity analysis correlating Ras/Raf interaction in vitro to Raf activation in vivo. *Nat. Struct.
1210 Mol. Biol.* **3**, 244–251 (1996).
- 1211 40. C. Herrmann, G. A. Martin, A. Wittinghofer, Quantitative Analysis of the Complex between
1212 p21 and the Ras-binding Domain of the Human Raf-1 Protein Kinase. *J. Biol. Chem.* **270**,
1213 2901–2905 (1995).
- 1214 41. K. Scheffzek *et al.*, Structural analysis of the GAP-related domain from neurofibromin and
1215 its implications. *EMBO J.* **17**, 4313–4327 (1998).
- 1216 42. G. F. Xu *et al.*, The neurofibromatosis type 1 gene encodes a protein related to GAP. *Cell.*
1217 **62**, 599–608 (1990).
- 1218 43. M. Barbacid, ras Genes. *Annu. Rev. Biochem.* **56**, 779–827 (1987).
- 1219 44. K. Rajalingam, R. Schreck, U. R. Rapp, Š. Albert, Ras oncogenes and their downstream
1220 targets. *Biochim. Biophys. Acta BBA - Mol. Cell Res.* **1773**, 1177–1195 (2007).
- 1221 45. M. J. Smith, M. Ikura, Integrated RAS signaling defined by parallel NMR detection of
1222 effectors and regulators. *Nat. Chem. Biol.* **10**, 223–230 (2014).
- 1223 46. C. Jia, M. Qian, D. Jiang, Overshoot in biological systems modelled by Markov chains: a
1224 non-equilibrium dynamic phenomenon. *IET Syst. Biol.* **8**, 138–145 (2014).
- 1225 47. L. Wiesmüller, A. Wittinghofer, Expression of the GTPase activating domain of the
1226 neurofibromatosis type 1 (NF1) gene in Escherichia coli and role of the conserved lysine
1227 residue. *J. Biol. Chem.* **267**, 10207–10210 (1992).

- 1228 48. Q. Hong, Small Open Chemical Systems Theory: Its Implications to Darwinian Evolution
1229 Dynamics, Complex Self-Organization and Beyond. *Commun. Theor. Phys.* **62**, 550–554
1230 (2014).
- 1231 49. L. Von Bertalanffy, The theory of open systems in physics and biology. *Science*. **111**, 23–
1232 29 (1950).
- 1233 50. A. Fersht, *Structure and Mechanism in Protein Science: A Guide to Enzyme Catalysis and*
1234 *Protein Folding* (Macmillan, 1999).
- 1235 51. L. Janosi, Z. Li, J. F. Hancock, A. A. Gorfe, Organization, dynamics, and segregation of
1236 Ras nanoclusters in membrane domains. *Proc. Natl. Acad. Sci.* **109**, 8097–8102 (2012).
- 1237 52. S. J. Plowman, C. Muncke, R. G. Parton, J. F. Hancock, H-ras, K-ras, and inner plasma
1238 membrane raft proteins operate in nanoclusters with differential dependence on the actin
1239 cytoskeleton. *Proc. Natl. Acad. Sci.* **102**, 15500–15505 (2005).
- 1240 53. A. Fischer *et al.*, B- and C-RAF Display Essential Differences in Their Binding to Ras THE
1241 ISOTYPE-SPECIFIC N TERMINUS OF B-RAF FACILITATES RAS BINDING. *J. Biol.*
1242 *Chem.* **282**, 26503–26516 (2007).
- 1243 54. H. J. Motulsky, L. C. Mahan, The kinetics of competitive radioligand binding predicted by
1244 the law of mass action. *Mol. Pharmacol.* **25**, 1–9 (1984).
- 1245 55. A.-C. Butty *et al.*, A positive feedback loop stabilizes the guanine-nucleotide exchange
1246 factor Cdc24 at sites of polarization. *EMBO J.* **21**, 1565–1576 (2002).
- 1247 56. J. Gureasko *et al.*, Role of the histone domain in the autoinhibition and activation of the
1248 Ras activator Son of Sevenless. *Proc. Natl. Acad. Sci. U. S. A.* **107**, 3430–3435 (2010).
- 1249 57. G. Bollag *et al.*, Loss of NF1 results in activation of the Ras signaling pathway and leads to
1250 aberrant growth in haematopoietic cells. *Nat. Genet.* **12**, 144–148 (1996).
- 1251 58. J. E. Toettcher, O. D. Weiner, W. A. Lim, Using Optogenetics to Interrogate the Dynamic
1252 Control of Signal Transmission by the Ras/Erk Module. *Cell.* **155**, 1422–1434 (2013).
- 1253 59. S. Ghosh, R. M. Bell, Regulation of Raf-1 kinase by interaction with the lipid second
1254 messenger, phosphatidic acid. *Biochem. Soc. Trans.* **25**, 561–565 (1997).
- 1255 60. A. K. Freeman, D. A. Ritt, D. K. Morrison, The importance of Raf dimerization in cell
1256 signaling. *Small GTPases*. **4**, 180–185 (2013).
- 1257 61. D. F. Brennan *et al.*, A Raf-induced allosteric transition of KSR stimulates phosphorylation
1258 of MEK. *Nature*. **472**, 366–369 (2011).
- 1259 62. D. A. Ritt, I. O. Daar, D. K. Morrison, KSR regulation of the Raf-MEK-ERK cascade.
1260 *Methods Enzymol.* **407**, 224–237 (2006).
- 1261 63. S. J. Leavers, H. F. Paterson, C. J. Marshall, Requirement for Ras in Raf activation is
1262 overcome by targeting Raf to the plasma membrane. *Nature*. **369**, 411–414 (1994).

- 1263 64. J. P. Wynne *et al.*, Rap1-interacting adapter molecule (RIAM) associates with the plasma
1264 membrane via a proximity detector. *J. Cell Biol.* **199**, 317–330 (2012).
- 1265 65. S. J. Cook, B. Rubinfeld, I. Albert, F. McCormick, RapV12 antagonizes Ras-dependent
1266 activation of ERK1 and ERK2 by LPA and EGF in Rat-1 fibroblasts. *EMBO J.* **12**, 3475–
1267 3485 (1993).
- 1268 66. X. Zhang, J. Gureasko, K. Shen, P. A. Cole, J. Kuriyan, An Allosteric Mechanism for
1269 Activation of the Kinase Domain of Epidermal Growth Factor Receptor. *Cell.* **125**, 1137–
1270 1149 (2006).
- 1271 67. Y. Wu, J. Vendome, L. Shapiro, A. Ben-Shaul, B. Honig, Transforming binding affinities
1272 from 3D to 2D with application to cadherin clustering. *Nature.* **475**, 510–513 (2011).
- 1273 68. K. A. Johnson, Z. B. Simpson, T. Blom, Global kinetic explorer: a new computer program
1274 for dynamic simulation and fitting of kinetic data. *Anal. Biochem.* **387**, 20–29 (2009).

1275

1276 **Figure Legends**

1277 **Figure 1. Multiple activities that are frequently perturbed in disease dynamically regulate**
1278 **Ras activity to control the assembly of downstream effectors during signal processing.**
1279 (a) Depiction of the proximal architecture of Ras signaling systems. Ras is activated by guanine
1280 exchange factors (GEFs) that exchange GDP for GTP and is inactivated by GTPase activating
1281 proteins (GAPs) that accelerate the hydrolysis of GTP. Activated Ras interacts with downstream
1282 effectors such as Raf or PI3 Kinase to assemble signaling complexes and elicit signaling
1283 outputs. (b) Abstraction of the proximal biochemical machinery underlying Ras processing of
1284 inputs into outputs, raising the question as to how the network configuration shapes signaling to
1285 multiple effector outputs.

1286

1287 **Figure 2. A network-level multi-turnover reconstitution of dynamic signal transmission**
1288 **from Ras to downstream effectors.** (a) Bead-based approach used to study how Ras systems
1289 assemble effector complexes in response to inputs. By incubating Ni-NTA microspheres that
1290 have been loaded with Ras in solutions containing GEFs, GAPs, and fluorescent effectors,
1291 system outputs can be observed by monitoring the accumulation of effector on the bead-bound
1292 Ras. (b) Example of GEF-catalyzed GTP-dependent translocation of fluorescent effector to Ras
1293 loaded bead. The amount of fluorescent effector bound to an individual bead before or after (10
1294 min) addition of 2 μM GEF +/- 5 mM GDP or GTP is shown. (c) Schematic depicting

1295 multiplexed assay workflow in which the output dynamics for many different system
1296 configurations can be measured by microscopy. (c) Dose dependent signaling response of
1297 effector translocation in response to increasing amounts of indicating RasGRF GEF activity. (d)
1298 Dose-dependent turn-off of output in the presence of saturating effector and increasing amounts
1299 of indicated NF1 GAP activity. (e) Combined turn on and turn off behavior of effector response
1300 when the system was activated with 2 μ M RasGRF GEF and after 30 min NF1-GAP was added.

1301 *The following figure supplements are available for this figure:*

1302 ***Figure 2-figure supplement 1. RasGRF GEF and NF1 GAP dose-dependent effects
1303 on effector output behaviors.***

1304

1305 **Figure 3. The extent of signal processing distortion by oncogenic alleles of Ras depends
1306 on the balance of positive and negative regulatory activities in the network.** (a) Depiction
1307 of wildtype Ras and oncogenic G12V Ras, illustrating the modes by which mutation is thought to
1308 impact the network behavior: changing in intrinsic hydrolysis rate, blocking GAP mediated
1309 hydrolysis, and modulating effector interactions. (b) Absolute and normalized effector responses
1310 to a 2 μ M RasGRF GEF step input in the absence of any GAP activity. (c) Absolute and
1311 normalized responses of the same step input as in (b), but with 1 μ M NF1 GAP activity present
1312 in the network. (d) Experimentally determined phase diagram derived from 16 output responses
1313 showing the magnitude of signal distortion caused by G12V substitution (defined as fold-change
1314 in integrated signal of G12V relative to wildtype) in different GEF and GAP network
1315 configurations.

1316 *The following figure supplements are available for this figure:*

1317 ***Figure 3-figure supplement 1. The extent of signal processing distortion by
1318 oncogenic G12C and Q61L alleles of Ras depends on the balance of positive and
1319 negative regulatory activities in the network.***

1320 ***Figure 3-figure supplement 2. Kinetic modeling and simulations suggest
1321 competition and intermediate GTPase states contribute to transient system
1322 behavior.***

1323

1324 **Figure 4. The concentration and identity of each Ras network component can modulate**
1325 **the timing, duration, shape, or amplitude of effector outputs.** (a) Depiction of the
1326 experimental setup: a fixed step-input is applied to a panel of Ras signaling systems in which
1327 the concentration of a single network component is varied to determine how each network
1328 component individually modulates system output. (b) Absolute and normalized effector
1329 responses to step-input in the presence of increasing amounts of the NF1 gap. (c) Absolute and
1330 normalized effector responses to step-input in the presence of increasing amounts of the p120
1331 GAP. (d) Absolute and normalized responses to step-input in the presence of different densities
1332 of Ras on the bead surface. (e) Absolute and normalized responses to step-input in the
1333 presence of increasing amounts of the C-Raf RBD effector.

1334

1335 **Figure 5. Tuning the levels of GEF, GAP, and GTPase provide access to a rich and**
1336 **diverse space of possible Ras signal processing behaviors.** (a) Depiction of the
1337 experimental setup: 4 different inputs (changes in apparent GEF activity) are applied to a panel
1338 of Ras signaling systems sampling 4 different p120GAP concentrations and 6 different Ras
1339 densities resulting in experimentally determined output responses for 96 different system
1340 configurations. (b) Experimentally determined absolute effector OUTPUT responses across 96
1341 different system configurations. Each graph corresponds to a particular GEF/GAP configuration,
1342 and each of the curves within that plot corresponds to a different Ras density as indicated by the
1343 color of the curve.

1344 *The following figure supplements are available for this figure:*

1345 ***Figure 5-figure supplement 1. Normalized (to maximum output) responses of***
1346 ***p120GAP/RasGRF/RafRBD/Ras signaling system under a variety of network***
1347 ***configurations.***

1348 ***Figure 5-figure supplement 2. Structure of RasGRF/p120GAP/H-Ras/cRaf response***
1349 ***space determined from outputs of 96 system configurations.***

1350 ***Figure 5-figure supplement 3. Kinetic modeling and simulations are consistent***
1351 ***with experimental observations about how system behavior is influenced by***
1352 ***network configuration.***

1353

1354 **Figure 6. Unique interpretation of Ras•GTP signals by different effectors in multi-effector**
1355 **networks encodes multiple distinct temporal outputs in the system response.** (a)
1356 Depiction of the experimental design: a fixed step-input is applied to a particular network
1357 configurations in which more than one effector molecule is, resulting in multiple simultaneous
1358 system outputs that are measured. (b) Absolute and normalized responses to step-input of C-
1359 Raf RBD and B-Raf RBD in the absence of any GAP activity. (c) as in (b) but with 1 μ M NF1-
1360 GAP present in the signaling network. (d) Absolute and normalized responses to step-input of
1361 C-Raf RBD and A-Raf RBD with 1 μ M NF1-GAP present in the signaling network. (e) Absolute
1362 and normalized responses to step-input of C-Raf RBD and the C-Raf^{N64A} mutant RBD with 1 μ M
1363 NF1-GAP present in the signaling network.

1364 *The following figure supplement is available for this figure:*

1365 ***Figure 6-figure supplement 1. Additional examples of how the unique***
1366 ***interpretation of Ras•GTP signals by different effectors in multi-effector networks***
1367 ***encodes multiple distinct temporal outputs in the system response.***

1368 ***Figure 6-figure supplement 2. Kinetic modeling and simulations show that***
1369 ***competition between effectors allows multiple temporal responses to be encoded***
1370 ***in the system output.***

1371 **Figure 7. Introducing recruitment-based positive feedback into the Ras signaling network**
1372 **alters output dynamics and amplifies weak signals in high-GAP contexts.** (a) Illustration of
1373 Ras system that now includes recruitment-based positive feedback and the synthetic GEF
1374 (RasGRF-RBD) that was used to implement the feedback. (b) Experimentally determined
1375 absolute effector OUTPUT responses across 96 different system configurations. Each graph
1376 corresponds to a particular GEF/GAP configuration, and each of the curves within that plot
1377 corresponds to a different Ras density as indicated by the color of the curve. (c) Examples of
1378 output responses for systems under equivalent network configurations (Position 1 of Figure 7D)
1379 that do (purple line) or do not (grey line) contain recruitment-based feedback. (e) Phase
1380 diagram depicting the gain provided by recruitment-based feedback (defined as fold-increase in
1381 integrated signaling output) in different network configurations.

1382 *The following figure supplement is available for this figure:*

1383 ***Figure 7-figure supplement 1. Normalized (to maximum output) responses of***
1384 ***p120GAP/ RasGRF-RBD feedback /RafRBD/Ras signaling system under a variety***
1385 ***of network configurations.***

1386

1387 **Figure 8. Introducing allosteric-based positive feedback into the Ras signaling network**
1388 **reduces transient overshoot and smooths the OUTPUT dynamics.** (a) Illustration of Ras
1389 system that now includes allosteric-based positive feedback and the naturally occurring GEF
1390 (SOScat) that was used to implement the feedback. (b) Experimentally determined absolute
1391 effector OUTPUT responses across 96 different system configurations. Each graph corresponds
1392 to a particular GEF/GAP configuration, and each of the curves within that plot corresponds to a
1393 different Ras density as indicated by the color of the curve. (c) Examples of output responses
1394 for systems under equivalent network configurations (high GEF, high GAP) that do (green line)
1395 or do not (grey line) contain allosteric feedback. (d) Schematic depiction of how an OFF->ON
1396 feedback mechanisms converts a step input in SOScat levels into a ramp input in SOScat
1397 activity.

1398 *The following figure supplement is available for this figure:*

1399 ***Figure 8-figure supplement 1. Normalized (to maximum output) responses of***
1400 ***p120GAP/ SOScat feedback /RafRBD/Ras signaling system under a variety of***
1401 ***network configurations.***

1402

1403

1404 **Figure 9. One system, many behaviors: versatility and fragility in the space of Ras**
1405 **GTPase signal processing behaviors.** (a) Illustration of direct and indirect diversity that exists
1406 in Ras network configurations. In the direct case, the distribution of p120GAP, H-Ras, and C-
1407 Raf gene expression levels across a variety of human cell-types are shown, synthesized from
1408 Genevestigator data (see associated Figure 9-source data 1). Each orange point corresponds to
1409 a cell-type and its position in the space indicates its associated expression level in each
1410 coordinate. A “shadow” of each point is projected onto each two-dimensional sub-plane to
1411 further clarify the distribution. In the indirect case, a schematic of two receptors that both
1412 activate Ras are indicated. One receptor results in strong recruitment of both GEF and GAP,
1413 while another only strongly recruits GEF. (b) Illustration depicting the versatility of Ras GTPase
1414 signaling systems. A simple step-input can be processed into a variety of different dynamic

1415 outputs depending on the network configuration. The way in which each network component
1416 shapes signaling is illustrated. (c) Illustration depicting the fragility of Ras GTPase signaling
1417 systems. Given a particular signaling output and a higher level disease output, there exist many
1418 paths by which the network configuration can change to produce the diseased output.

1419

1420 **VideoLegends**

1421 **Video1. Response of wildtype and G12V Ras systems in GAP-free network context.** The
1422 effector output (red) from a representative bead loaded with wildtype Ras (blue) or G12V Ras
1423 (green) is shown. 2 μ M RasGRF was provided as an activating input. Time-steps are separated
1424 by 15 minutes. Associated with data in main-text Figure 3B.

1425

1426 **Video2. Response of wildtype and G12V Ras systems in high-GAP network context.** The
1427 effector output (red) from a representative bead loaded with wildtype Ras (blue) or G12V Ras
1428 (green) is shown. 2 μ M RasGRF was provided as an activating input and the system contained
1429 1 μ M NF1-GAP. Time-steps are separated by 15 minutes. Associated with data in main-text
1430 Figure 3C.

1431

1432 **Table Legends**

1433 **Table 1. List of plasmids used this study.** A description of each construct used in this study,
1434 the bacterial antibiotic resistance associated with that plasmid, and a pSC reference index to
1435 facilitate any plasmid requests.

1436

1437 **Figure Supplement Legends**

1438 **Figure 2-figure supplement 1. RasGRF GEF and NF1 GAP dose-dependent effects on
1439 effector output behaviors.** (a) Dose-dependent effect of increasing RasGRF GEF
1440 concentrations on *initial rates* of the c-Raf RBD effector to Ras-loaded beads. (b) Dose-
1441 dependent effect of increasing RasGRF GEF concentrations on *steady state* levels of the c-Raf

1442 RBD effector on Ras-loaded beads. (c) Dose-dependent effect of increasing NF1 GAP
1443 concentrations on disappearance of c-Raf RBD effector from Ras•GTP-loaded beads

1444

1445 **Figure 3-figure supplement 1. The extent of signal processing distortion by oncogenic**
1446 **G12C and Q61L alleles of Ras depends on the balance of positive and negative**
1447 **regulatory activities in the network.** (a) Depiction of wildtype Ras and oncogenic G12C/Q61L
1448 Ras illustrating the modes by which mutation is thought to impact the network behavior:
1449 changing in intrinsic hydrolysis rate, blocking GAP mediated hydrolysis, and modulating effector
1450 interactions. (b) Absolute effector responses for G12C and WT Ras in response to a 2 μ M
1451 RasGRF GEF step input in the absence of any GAP activity. (c) As in (b) but with 1 μ M NF1
1452 GAP activity present in the network. (d) Absolute effector responses for Q61L and WT Ras in
1453 response to a 2 μ M RasGRF GEF step input in the absence of any GAP activity. (e) As in (d)
1454 but with 1 μ M NF1 GAP activity present in the network.

1455

1456 **Figure 3-figure supplement 2. Kinetic modeling and simulations suggest competition and**
1457 **intermediate GTPase states contribute to transient system behavior.** Kintek simulations for
1458 a variety of models. Each simulation contains initial conditions of 50 nM effector, 10 nM GDP
1459 bound Ras, a GEF activity of \sim 1 μ M, and an “infinite” supply of nucleotide (100000 nM). (a)
1460 Output of Kintek simulation based on the simplest two-state model described in the main text
1461 methods. [GAP] is titrated by varying the hydrolysis rate constant over 5 orders of magnitude.
1462 (b) Output of Kintek simulation based on extending the simplest two-state model to include
1463 competition between GAP and effectors as described in the main text methods. The output from
1464 6 different GAP concentrations are shown for two different GAP parameter choices. Overshoot
1465 is observed for the non-physiologic GAP parameter set ($k_{off}=0.0001\text{ s}^{-1}$ and $k_{cat}=0.0001\text{ s}^{-1}$).
1466 However, this is not observed when physiologic GAP parameters are used ($k_{off}=0.01\text{ s}^{-1}$, $k_{cat}=1\text{s}^{-1}$).
1467 (c) Output from a 3-state GTPase model that includes competition between GAP and
1468 effector, as described in the main text methods. The output from 6 different GAP concentrations
1469 are shown for a physiologic choice of GAP parameters ($k_{off}=0.01\text{ s}^{-1}$, $k_{cat}=1\text{s}^{-1}$). Transient
1470 overshoot behavior mirroring the experimentally obtained data in Figure 3 are obtained in this
1471 simulation.

1472

1473 **Figure 5-figure supplement 1. Normalized (to maximum output) responses of**
1474 **p120GAP/RasGRF/RafRBD/Ras signaling system under a variety of network**
1475 **configurations.** Normalized (to the maximum output value of the response) signaling
1476 responses for different network GEF/GAP/Ras density configurations. The RasGRF catalytic
1477 domain was used as the activating GEF in these experiments. The p120GAP catalytic domain
1478 was used as the GAP in these experiments. 50 nM cRaf-RBD was used as the effector in these
1479 experiments. The response for differing densities of Ras in each GEF/GAP configuration is
1480 shown by different color lines in each plot, with estimated densities indicated in the key.

1481

1482 **Figure 5-figure supplement 2. Structure of RasGRF/p120GAP/H-Ras/cRaf response space**
1483 **determined from outputs of 96 system configurations.** Phase diagrams for three different
1484 output features—integrated signal, initial rate of response, and overshoot behavior—at three
1485 different Ras density levels, constructed by interpolating these output features from the 96
1486 responses shown in Figure 5B.

1487

1488 **Figure 5-figure supplement 3. Kinetic modeling and simulations are consistent with**
1489 **experimental observations about how system behavior is influenced by network**
1490 **configuration.** (a) Output of Kintek simulation using a 3-state GTPase model with competition
1491 between GAP and effectors as described in the main-text Materials and methods, in which the
1492 Ras density (i.e. concentration in this model) is varied over 4 orders of magnitude as indicated.
1493 Initial conditions were 50 nM effector, 1 uM GEF, no GAP and infinite nucleotide (100000 nM).
1494 The model recovers the observation that at low densities, more transient behavior is observed
1495 than at high Ras densities, which show a more associative response. (b) Output of Kintek
1496 simulation using a 3-state GTPase model with competition between GAP and effectors as
1497 described in the main-text Materials and methods, in which GAP parameter choices that
1498 resemble the NF1-GAP ($k_{off}=0.01\text{s}^{-1}$, $k_{cat}=0.1\text{s}^{-1}$) or p120GAP ($k_{off}=0.25\text{s}^{-1}$, $k_{cat}=0.4\text{s}^{-1}$) are used.
1499 Initial conditions were 50 nM effector, 10 nM Ras, 1 uM GEF, 1 uM GAP and infinite nucleotide
1500 (100000 nM). This model recovers the observation that differences in Km and kcat can result in
1501 equivalent amounts of NF1gap and p120GAP producing different transient behaviors in the
1502 system output. (c) Output of Kintek simulation using a 3-state GTPase model with competition
1503 between GAP and effectors as described in the main-text Materials and methods, in which
1504 effector concentrations are varied over 5 orders of magnitude. Initial conditions were 10 nM Ras,

1505 1 uM GEF, no GAP and infinite nucleotide (100000 nM). This model recovers the observation
1506 that higher effector concentrations allow more transient features of the time-varying GTPase
1507 signal to be captured in the system output.

1508

1509 **Figure 6-figure supplement 1. Additional examples of how the unique interpretation of**
1510 **RasGTP signals by different effectors in multi-effector networks encodes multiple**
1511 **distinct temporal outputs in the system response.** (a) Depiction of the experimental design:
1512 a fixed step-input is applied to a particular network configurations in which more than one
1513 effector molecule is, resulting in multiple simultaneous system outputs that are measured. (b)
1514 Absolute and normalized responses to step-input of C-Raf RBD and A-Raf RBD in the absence
1515 of any GAP activity. (c) Absolute and normalized responses to step-input of C-Raf RBD and C-
1516 Raf^{N64A} RBD in the absence of any GAP activity.

1517

1518 **Figure 6-figure supplement 2. Kinetic modeling and simulations show that competition**
1519 **between effectors allows multiple temporal responses to be encoded in the system**
1520 **output.** (a) Output of Kintek simulation using a 3-state GTPase model with competition between
1521 GAP and effectors as described in the main-text Materials and methods, in which two effectors
1522 (one c-Raf like ($k_{off}=0.001$ s⁻¹), one B-Raf like ($k_{off}= 0.00025$ s⁻¹) are present in the system at
1523 50 nM. Other initial conditions were 50 nM effector, 1 uM GEF, 1 uM GAP and infinite nucleotide
1524 (100000 nM). This simulation recovers the observation that B-Raf can respond in a sustained
1525 way while C-Raf can respond in a transient way. (b) Output of Kintek simulation using a 3-state
1526 GTPase model with competition between GAP and effectors as described in the main-text
1527 Materials and methods, in which two effectors have very similar concentrations and parameters
1528 (as indicated on the figure). Other initial conditions were 50 nM effector, 1 uM GEF, 1 uM GAP
1529 and infinite nucleotide (100000 nM). This simulation recovers the observation that small
1530 parameter differences between effector can alter the timing and duration of transient signaling
1531 outputs. (c) Output of Kintek simulation using a 3-state GTPase model with competition between
1532 GAP and effectors as described in the main-text Materials and methods, in which three effectors
1533 with different parameters and concentrations (as indicated in the figure) are present in the
1534 system. Other initial conditions were 50 nM effector, 1 uM GEF, 1 uM GAP and infinite
1535 nucleotide (100000 nM). This simulation shows that a complex sequence of effector outputs can
1536 be produced (3 THEN 2 THEN 1) in response to a step input simply by titration of levels and
1537 altering effector parameters.

1538

1539 **Figure 7-figure supplement 1. Normalized (to maximum output) responses of p120GAP/**
1540 **RasGRF-RBD feedback /RafRBD/Ras signaling system under a variety of network**
1541 **configurations.** Normalized (to the maximum output value of the response) signaling
1542 responses for different network GEF/GAP/Ras density configurations. The recruitment-based
1543 positive feedback GEF RasGRF-RBD was used as the activating GEF in these experiments.
1544 The p120GAP catalytic domain was used as the GAP in these experiments. 50 nM cRaf-RBD
1545 was used as the effector in these experiments. The response for differing densities of Ras in
1546 each GEF/GAP configuration is shown by different color lines in each plot, with estimated
1547 densities indicated in the key.

1548

1549 **Figure 8-figure supplement 1. Normalized (to maximum output) responses of p120GAP/**
1550 **SOScat feedback /RafRBD/Ras signaling system under a variety of network**
1551 **configurations.**

1552 Normalized (to the maximum output value of the response) signaling responses for different
1553 network GEF/GAP/Ras density configurations. The allosteric-based positive feedback GEF
1554 SOScat was used as the activating GEF in these experiments. The p120GAP catalytic domain
1555 was used as the GAP in these experiments. 50 nM cRaf-RBD was used as the effector in these
1556 experiments. The response for differing densities of Ras in each GEF/GAP configuration is
1557 shown by different color lines in each plot, with estimated densities indicated in the key.

1558

1559 **Source Data Legends**

1560 **Figure 9-source data 1. Relative gene expression level data from a variety of human**
1561 **tissue and cell types that was used to produce the plot in Figure 8A.**

1562 This table contains the relative expression-level data that was used to prepare the plot in Figure
1563 9A. These data were obtained from Genevestigator as outlined in the main-text Materials and
1564 methods.

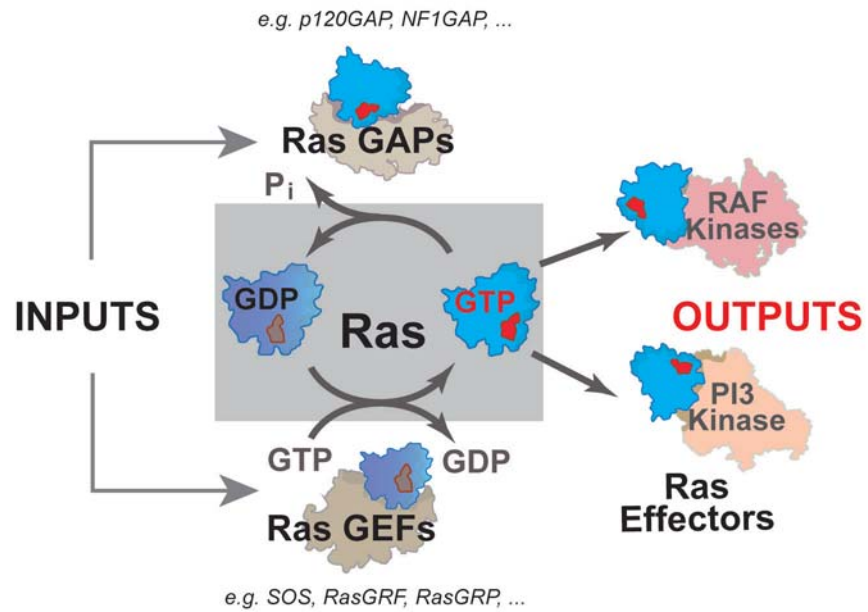
1565

1566

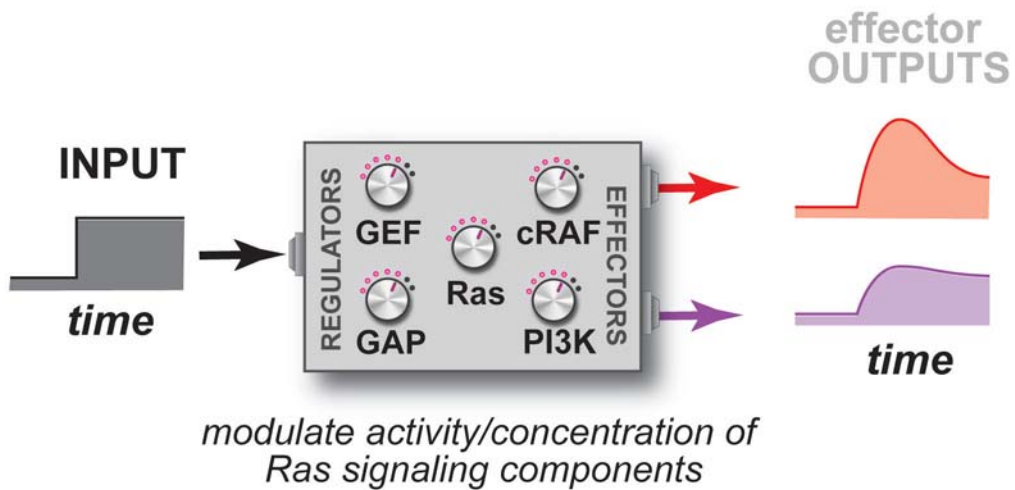
1567

1568

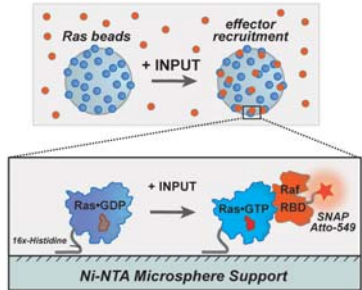
A



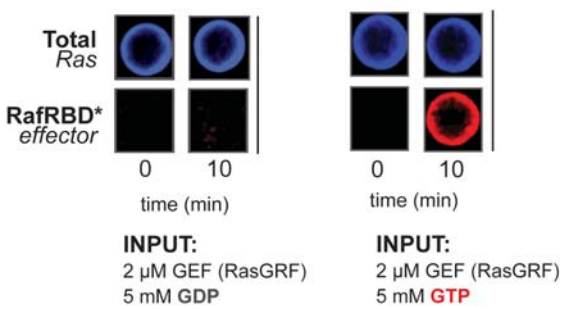
B



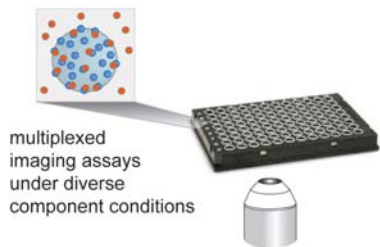
A on-bead reconstitution of Ras signal transmission



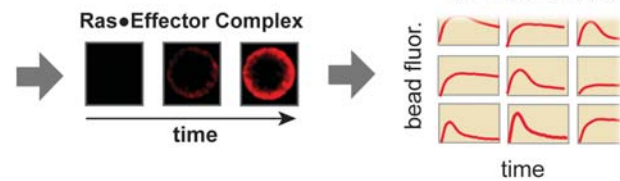
B GTP-dependent translocation of effector to bead



C

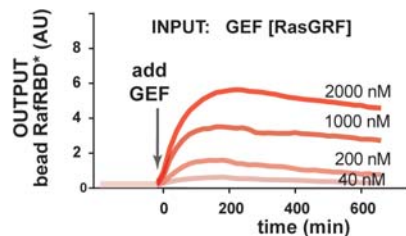
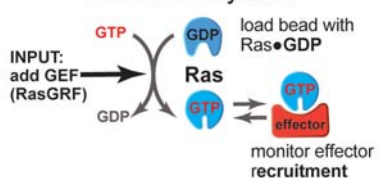


Assay Workflow



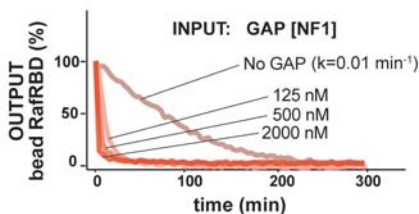
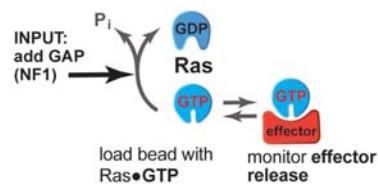
D

TURN ON system



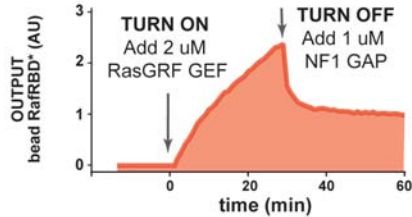
E

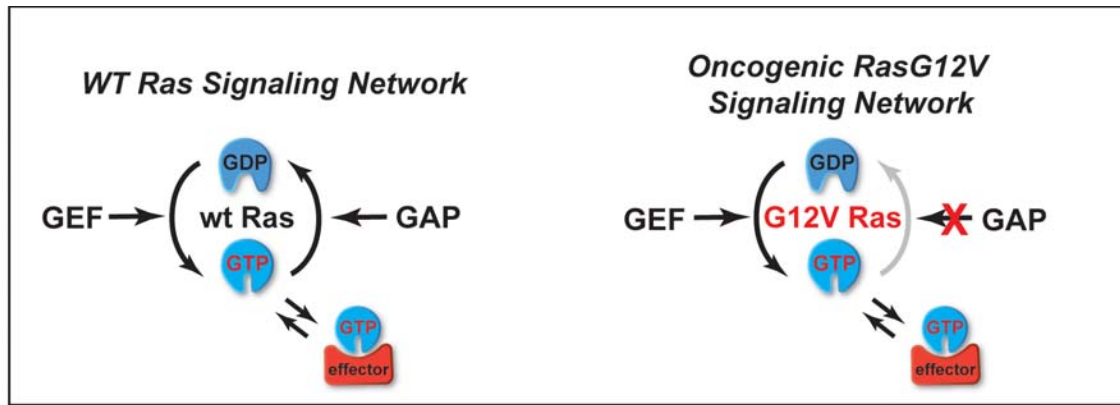
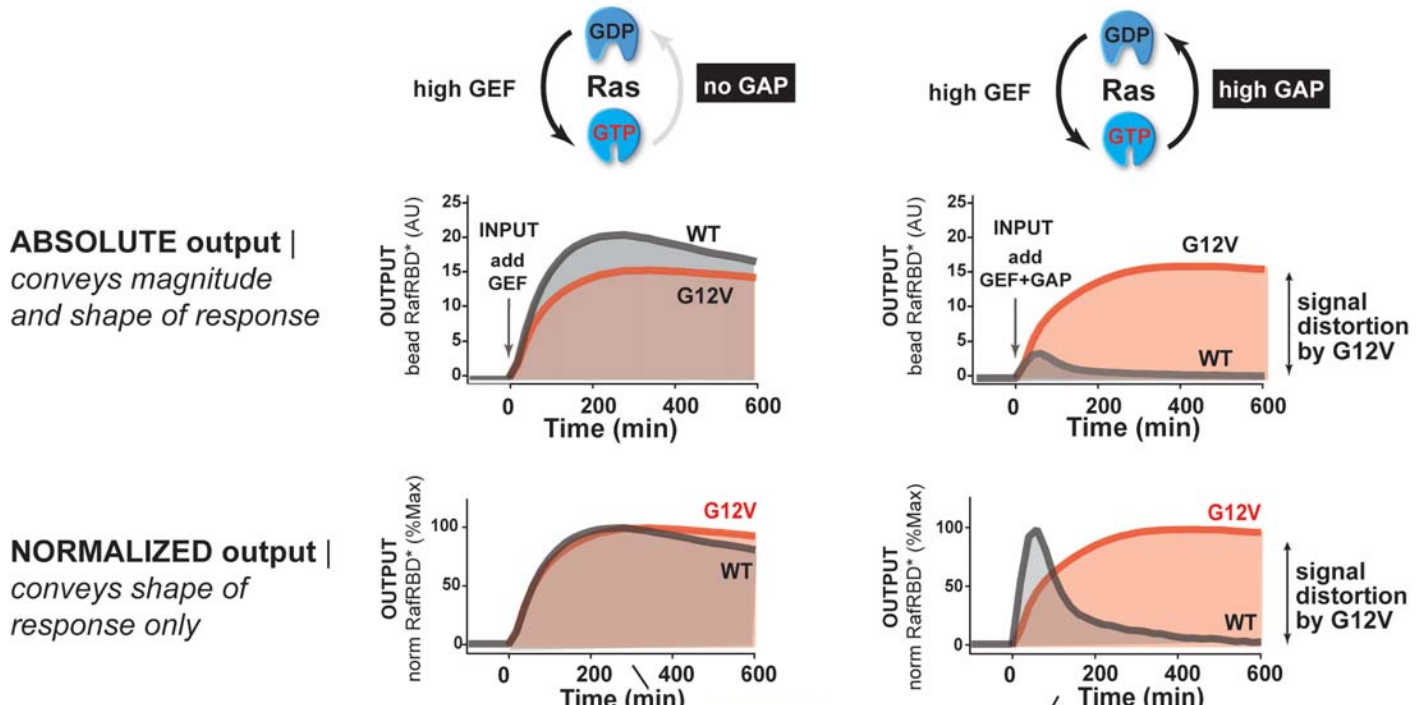
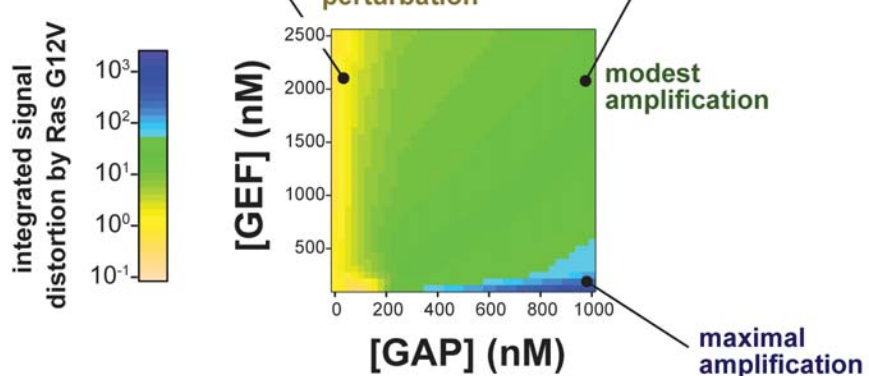
TURN OFF system

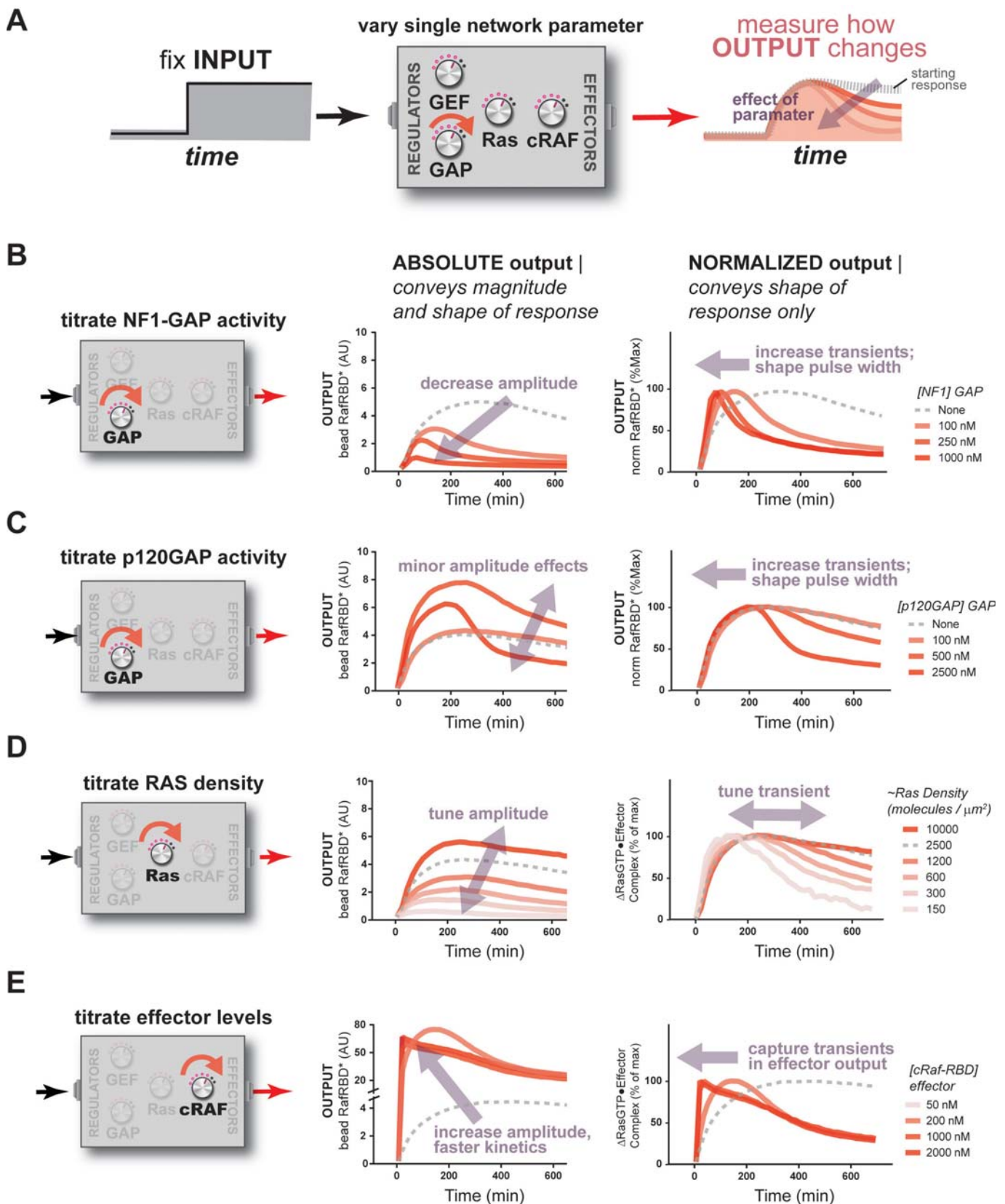


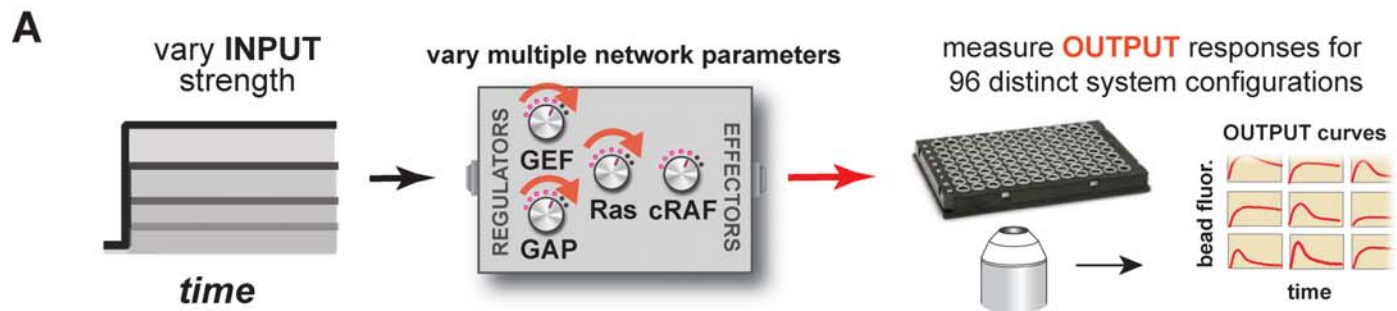
F

combined TURN ON and TURN OFF of system



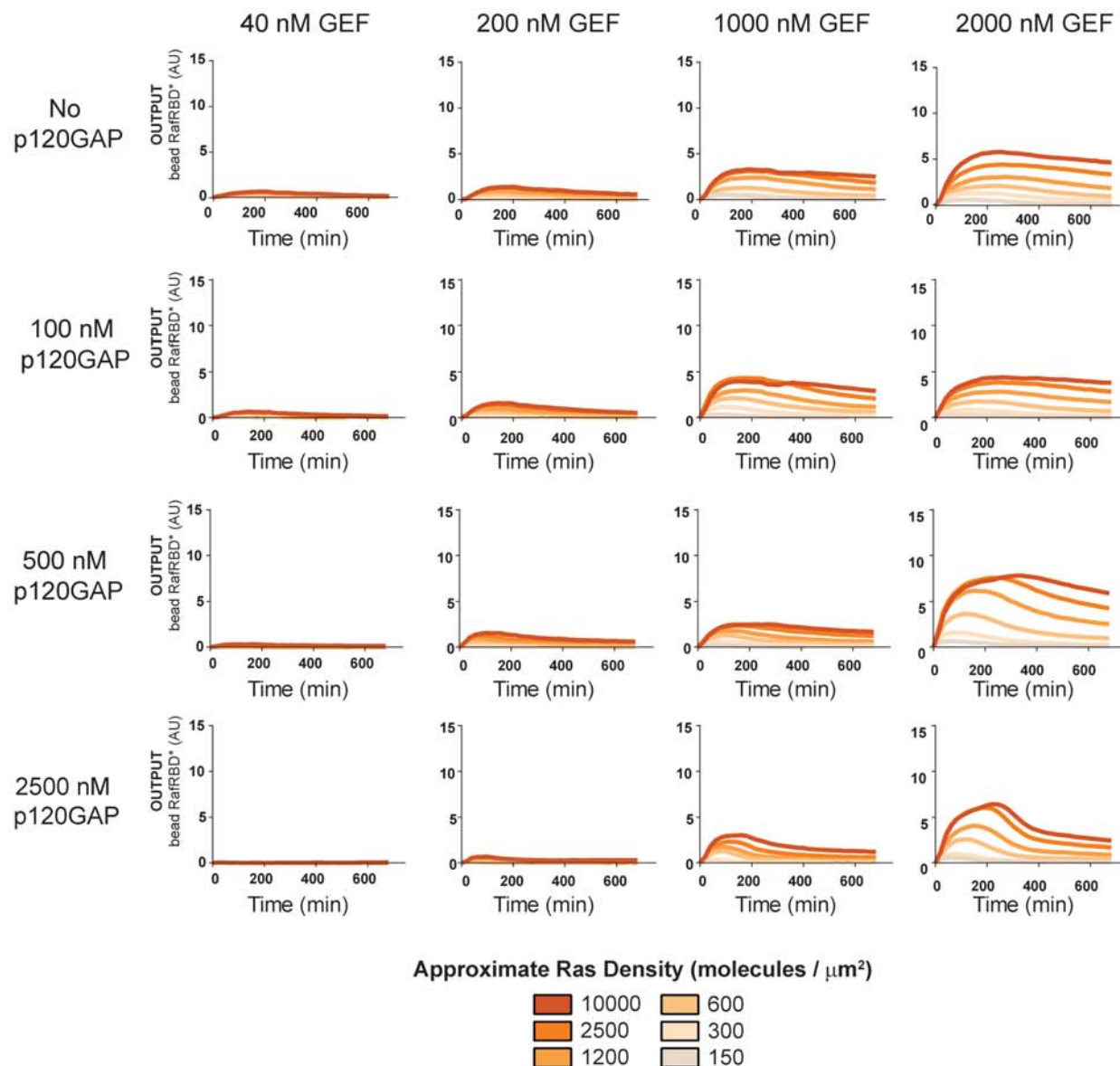
A**B****D**





B

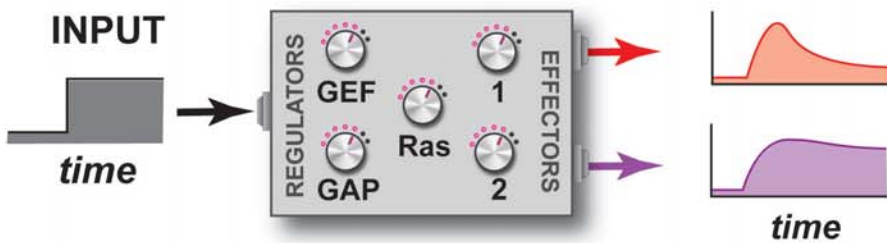
Experimental effector OUTPUT responses in different GEF, GAP, and Ras configurations



A

Multi-Effector Ras Signaling Network

measure multiple
OUTPUTS

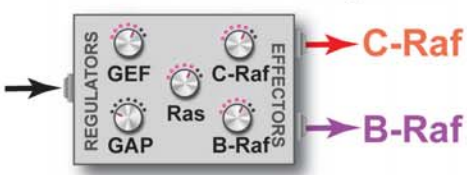


Effector 1

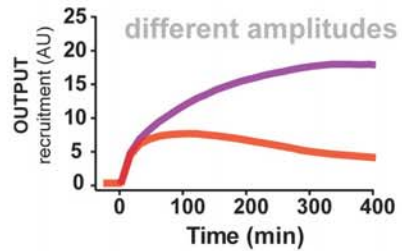
Effector 2

B

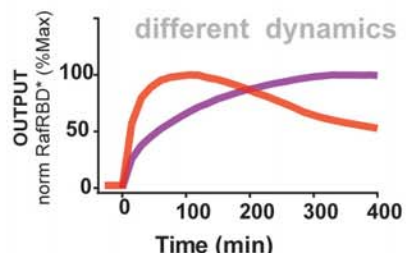
no GAP network configuration



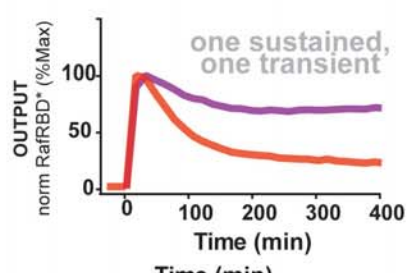
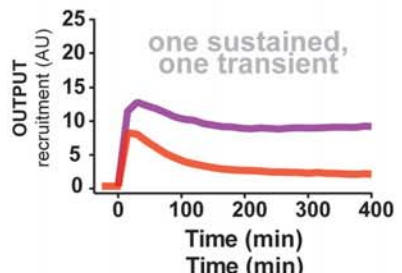
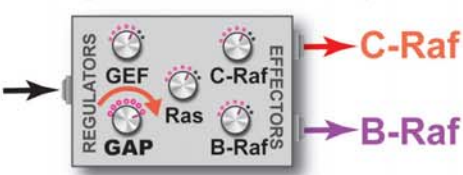
ABSOLUTE output |
conveys magnitude
and shape of response



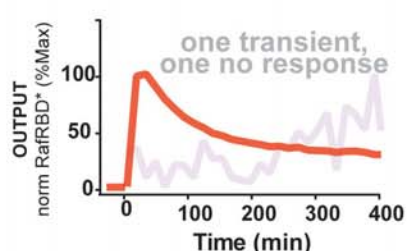
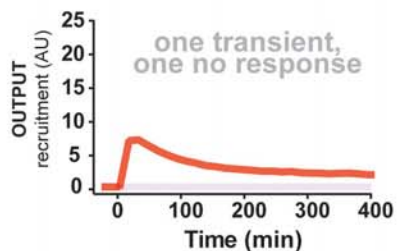
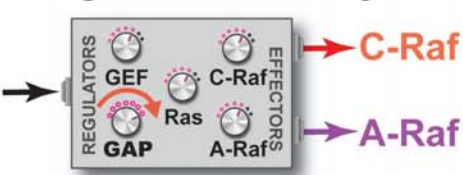
NORMALIZED output |
conveys shape of
response only

**C**

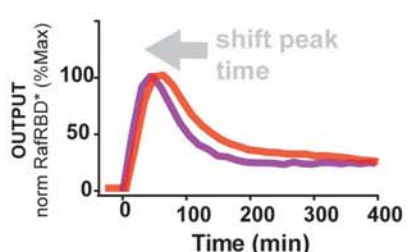
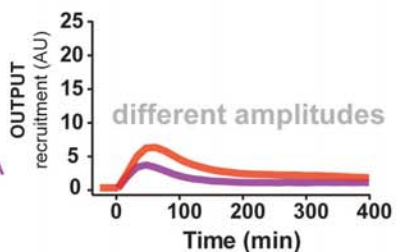
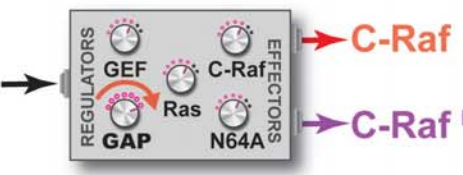
high GAP network configuration

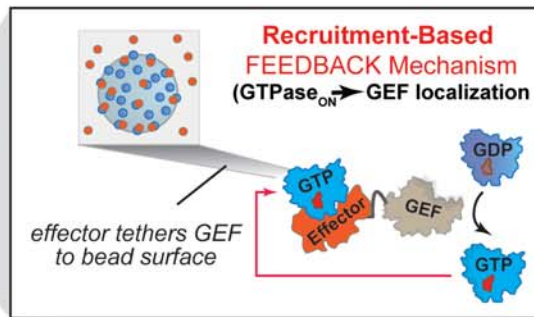
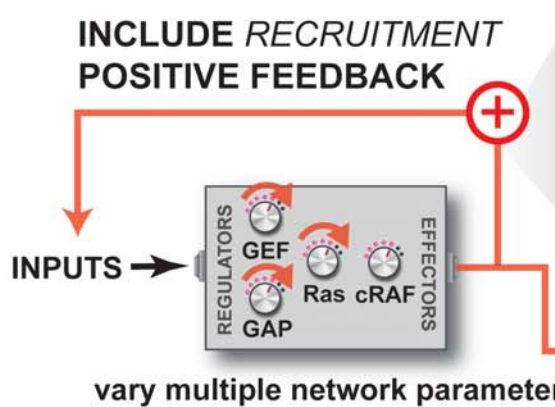
**D**

high GAP network configuration

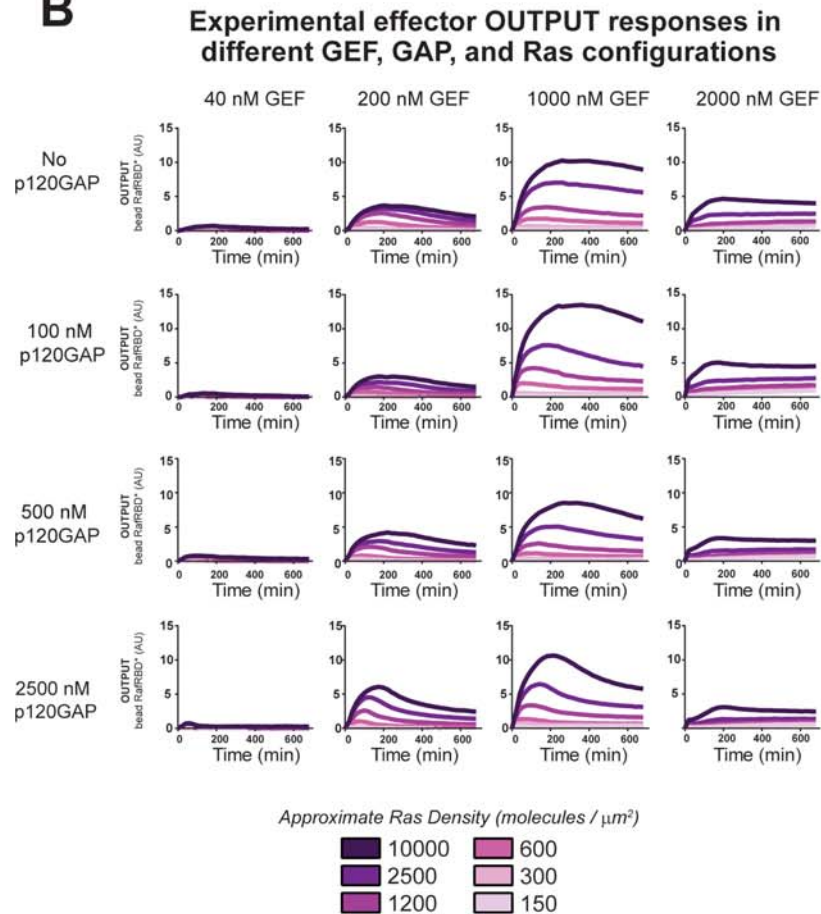
**E**

high GAP network configuration

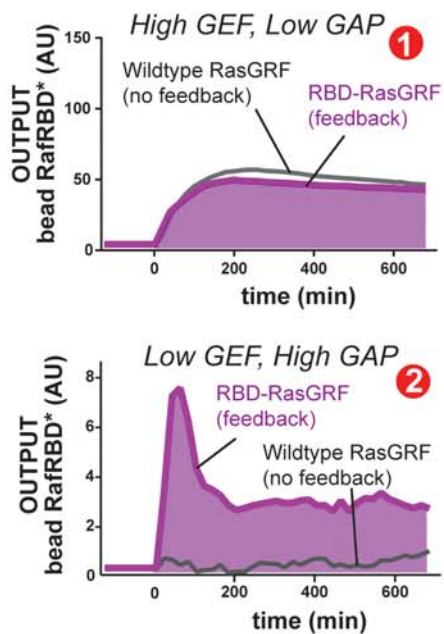


A

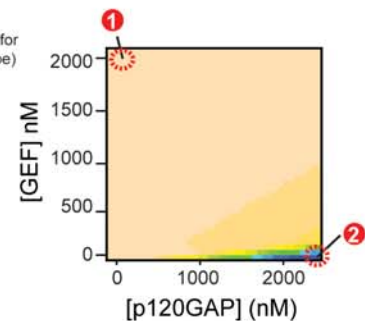
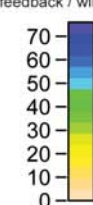
measure **OUTPUT** responses for 96 distinct system configurations in the presence of FEEDBACK

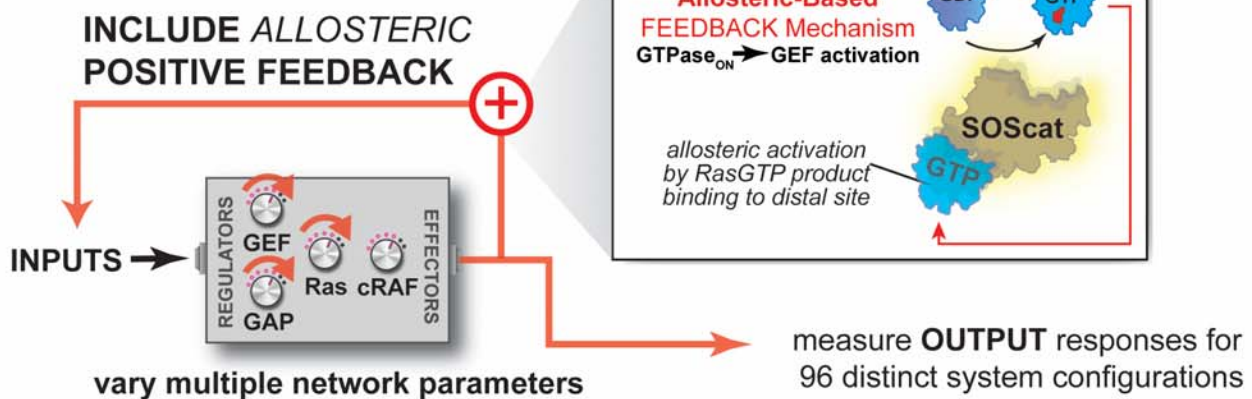
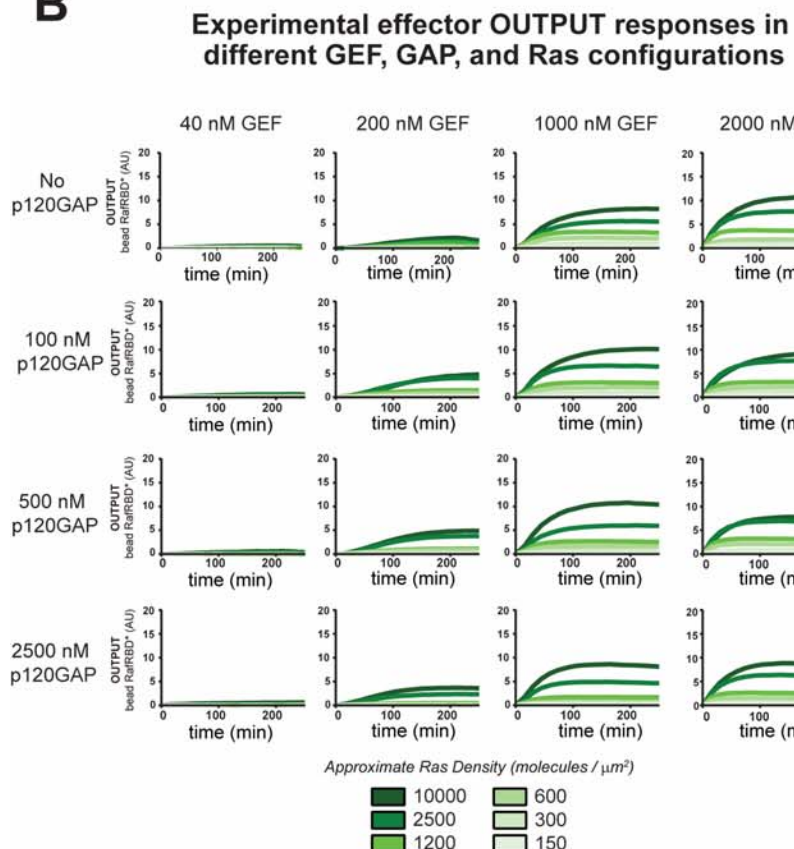
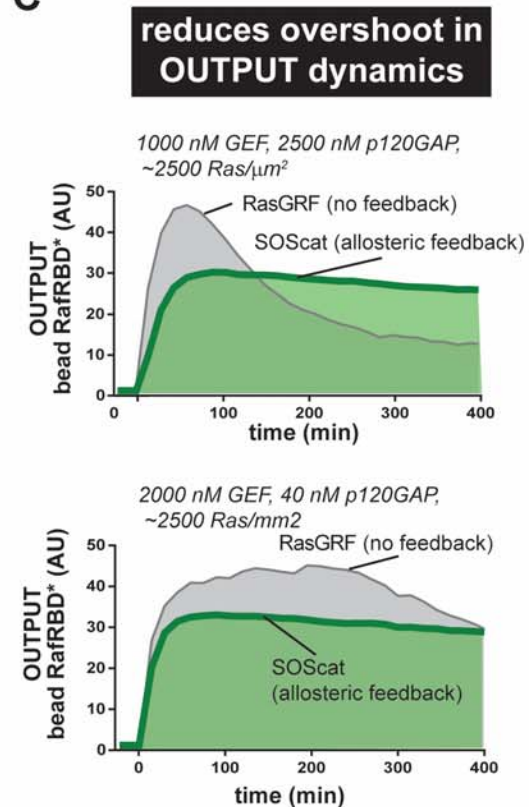
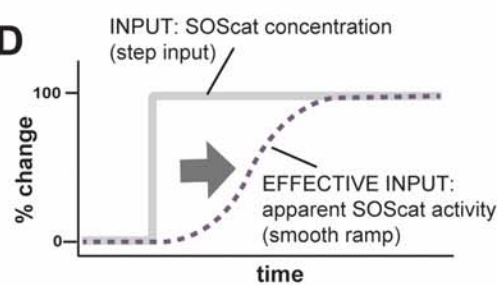
B**C**

**amplifies weak signals
in high GAP contexts**

**D**

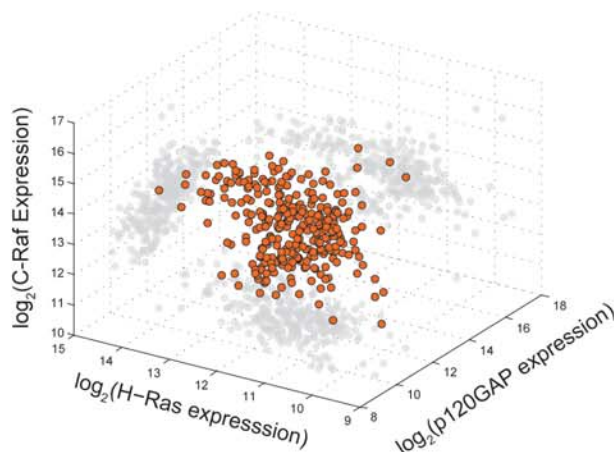
**Feedback
Gain**
(integrated signal for feedback / wildtype)



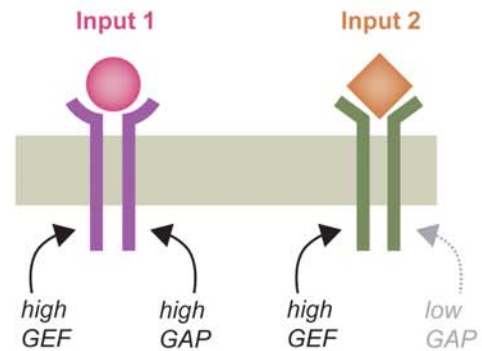
A**B****C****D**

A Ras network configurations are highly diverse across different cell-types and stimuli

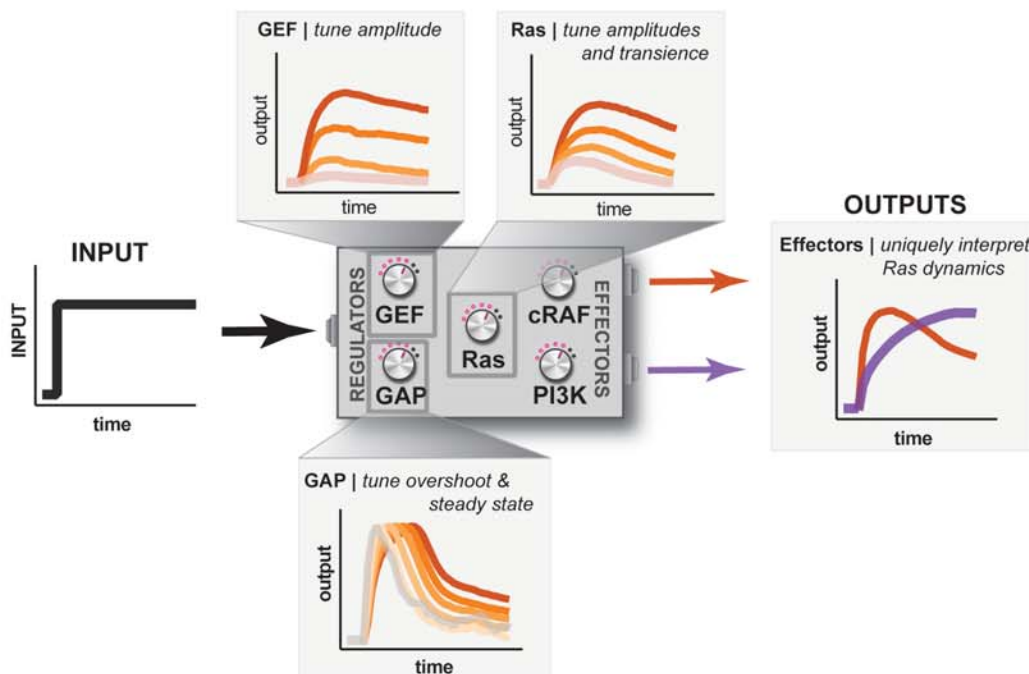
DIRECT | expression levels of components



INDIRECT | effective concentrations via how receptors recruit activities



B VERSATILITY | a programmable space of diverse multi-output dynamic signaling outcomes



C FRAGILITY | multiple failure points and paths to undesirable signaling outcomes and disease

